Atmos. Chem. Phys., 9, 3641–3662, 2009
www.atmos-chem-phys.net/9/3641/2009/

Atmospheric Chemistry and Physics

Tropospheric NO_2 column densities deduced from zenith-sky DOAS measurements in Shanghai, China, and their application to satellite validation

D. Chen[1], **B. Zhou**[1], **S. Beirle**[2], **L. M. Chen**[1], **and T. Wagner**[2]

[1]Department of Environmental Science & Engineering, Fudan University, Shanghai, China
[2]Max-Planck-Institute for Chemistry, Mainz, Germany

Received: 20 June 2008 – Published in Atmos. Chem. Phys. Discuss.: 3 September 2008
Revised: 28 April 2009 – Accepted: 29 April 2009 – Published: 5 June 2009

Abstract. Zenith-sky scattered sunlight observations using differential optical absorption spectroscopy (DOAS) technique were carried out in Shanghai, China (31.3° N, 121.5° E) since December 2006. At this polluted urban site, the measurements provided NO_2 total columns in the daytime. Here, we present a new method to extract time series of tropospheric vertical column densities (VCDs) of NO_2 from these observations. The derived tropospheric NO_2 VCDs are important quantities for the estimation of emissions and for the validation of satellite observations. Our method makes use of assumptions on the relative NO_2 height profiles and the diurnal variation of stratospheric NO_2 VCDs. The main error sources arise from the uncertainties in the estimated stratospheric slant column densities (SCDs) and the determination of tropospheric NO_2 air mass factor (AMF). For a polluted site like Shanghai, the accuracy of our method is conservatively estimated to be $<$25% for solar zenith angle (SZA) lower than 70°. From simultaneously performed long-path DOAS measurements, the NO_2 surface concentrations at the same site were observed and the corresponding tropospheric NO_2 VCDs were estimated using the assumed seasonal NO_2 profiles in the planetary boundary layer (PBL). By making a comparison between the tropospheric NO_2 VCDs from zenith-sky and long-path DOAS measurements, it is found that the former provides more realistic information about total tropospheric pollution than the latter, so it's more suitable for satellite data validation. A comparison between the tropospheric NO_2 VCDs from ground-based zenith-sky measurements and SCIAMACHY was also made. Satellite validation for a strongly polluted area is highly needed, but exhibits also a great challenge. Our comparison shows good agreement, considering in particular the different spatial resolutions between the two measurements. Remaining systematic deviations are most probably related to the uncertainties of satellite data caused by the assumptions on aerosol properties as well as the layer heights of aerosols and NO_2.

Correspondence to: B. Zhou
(binzhou@fudan.edu.cn)

1 Introduction

Nitrogen dioxide (NO_2) is one of the most important trace gases in tropospheric chemistry. It directly participates in the photochemical formation of tropospheric ozone and contributes locally to radiative forcing (Solomon et al., 1999). The main NO_x ($NO_2 + NO$) sources include both anthropogenic and natural emissions, such as fossil fuel combustion, biomass burning, lightning and soil emission. Considering the importance of NO_2 to human health and atmospheric chemistry, there have been many ground-based, air-borne and space-borne instruments carrying out NO_2 observations. In situ sampling using chemiluminescence technique has been adopted as a routine monitoring method to measure NO_2 concentrations near the ground. With the development of remote sensing techniques, especially the differential optical absorption spectroscopy (DOAS), the total amount of NO_2 in the atmosphere can be acquired either from space or ground. After the launch of ERS-2 in 1995, the global distribution of total and tropospheric NO_2 is mapped by the Global Ozone Monitoring Experiment (GOME) (Burrows et al., 1999b) which helps to improve the knowledge of atmospheric pollution and its transportation. Additional satellite instruments were launched since then, continuing the GOME time series: in 2002 the SCanning ImagingAbsorption spectroMeter for Atmospheric CHartographY (SCIAMACHY) was launched on ENVISAT (Bovensmann et al., 1999); in 2004 the Ozone Monitoring Instrument (OMI) was launched on AURA (Levelt and Noordhoek, 2002); in 2006 the first GOME-2 instrument (in total three instruments are scheduled) was launched on METOP (EUMETSAT, 2008).

Ground-based instruments (like e.g. Systeme d'Analyse par Observations Zenithales, SAOZ or similar UV/vis instruments) (see e.g. Noxon, 1975) installed at a number of NDACC stations over the globe continuously provide the total NO_2 columns for trend analysis and satellite data validation (Pommereau and Goutail, 1988; Ionov et al., 2006a). Moreover, as an advanced improvement of Zenith-sky DOAS, Multi AXis Differential Optical Absorption Spectroscopy (MAX-DOAS) instrument was developed to retrieve vertical profile of NO_2 concentrations, as well as tropospheric and stratospheric columns, so it is suitable for the validation of satellite tropospheric data (Hönninger and Platt, 2002; Heue et al., 2005; Celarier et al., 2008; Brinksma et al., 2008).

Richter et al. (2005) reported a significant increase of tropospheric NO_2 columns over East Central China from 1996–2004 observed by GOME and SCIAMACHY. By attributing such increase to the growth of NO_x emission, the authors pointed out the necessity of detailed inventory studies to confirm the satellite data. However, considering the sensitivity of satellite observations to pollution located near the ground, as well as the uncertainties contained in satellite retrieval process (Boersma et al., 2004), it seems necessary to carry out ground-based measurements of NO_2 surface concentrations and total tropospheric column densities in east central China to investigate the tropospheric pollution status and validate the satellite observations. Ground-based instruments can in particular yield additional valuable information on finer spatial scales and about the diurnal variation.

For this purpose, zenith-sky DOAS and long-path DOAS measurements were performed in Shanghai, China (31.3° N, 121.5° E). By combining these two observations, both the tropospheric columns and surface concentrations of NO_2 can be acquired. In contrast to previous studies, which measured only twilight NO_2 columns (e.g. Petritoli et al., 2004; Ionov et al., 2006b), the present study observed zenith-sky scattered light during the whole day and retrieved the diurnal variation of the total NO_2 columns. By using some simple but rational assumptions, the tropospheric NO_2 columns were extracted from the total ones. Such studies provide comprehensive information about surface emissions and total tropospheric pollution, which is necessary for satellite data validation and total emission investigation. A comparison between the two measurement results (zenith-sky and long-path DOAS) can also provide some indications about the diurnal variation of planetary boundary layer (PBL) height.

The paper is organized as follows: in the next chapter the two ground-based DOAS instruments (zenith-sky and long-path) are described. In Chap. 3, the determination of tropospheric NO_2 vertical columns from these observations is outlined. Chapter 4 presents a comparison between both ground-based data sets and finally with satellite observations.

2 Ground-based instruments and spectral analysis

2.1 Zenith-sky measurements

2.1.1 Instrument and experiments

Ground-based observations of zenith-sky scattered sunlight were firstly performed from 16 December 2006 to 18 December 2006 at Chongming Island (31.5° N, 121.8° E), which lies to the northeast of Shanghai on the Pacific Ocean, and is located at the estuary of Yangtze River. Considering the geographical location of this island and the few industries on it, it can be concluded as the most suitable rural site around Shanghai with small tropospheric NO_2 pollution. The recording of zenith-sky scattered sunlight was performed automatically when the solar zenith angle (SZA) was below 92°.

After the three-day experiment, the instruments were moved to Fudan University (31.3° N, 121.5° E), carrying out continuous ground-based measurements since 22 December 2006. Located near the middle circle viaduct of Shanghai, this urban site suffers from heavy traffic pollution. The NO_2 absorption signal can be easily detected in the spectra, in which the contribution of the tropospheric part is usually much larger than the stratospheric one, especially at small SZAs. The instrument mounted on the top roof stairs of a 20 m-tall building comprises three parts, including a telescope, a spectrometer and a PC. The scattered sunlight is received by a telescope with 46 mm diameter and 300 mm focal length, and led to spectrometer via a quartz fiber. The HR4000 high resolution fiber optic spectrometer (Ocean Optics, Inc.) is used to acquire UV-visible zenith-sky spectra with a 1200 grooves/mm grating and a 100 μm wide entrance slit, which yields a full-width half-maximum (FWHM) resolution of about 0.73 nm. The detector is a linear CCD array with 3648 pixels (each 8 μm×200 μm). A PC controls the automatic measurements and stores the spectra. The dark current and electronic offset are removed automatically during the spectra recording process. The signal of dark current is measured every night and subtracted from each spectrum according to the corresponding average exposure time. Depending on the intensity of the received scattered sunlight, the exposure time is adjusted automatically to maximize the total signal. Simultaneously, the number of accumulations comprising a spectrum also varies to restrict the average time interval between two spectra to about 5 min. The wavelength range is 345–565 nm.

2.1.2 NO_2 total column retrieval

The NO_2 column densities are retrieved by means of Differential Optical Absorption Spectroscopy (DOAS) (Platt, 1994), using the spectral region between 434 nm and 462 nm. The WinDOAS-software (Fayt and Roozendael, 2001) is applied to analyze the zenith-sky spectra. The logarithm of a Fraunhofer reference spectrum as well as several trace gas absorption cross sections are fitted to the logarithm of each measured spectrum by means of a non-linear least squares fitting routine (allowing shift and squeeze of the fitted spectra). The Fraunhofer reference spectrum is measured by the same instruments in a similar way as all other spectra, but taking into account two requirements to ensure that it contains a rather small NO_2 absorption: first it was measured during noon to minimize the stratospheric contribution; second it was measured during a day with little pollution (as concluded from simultaneous surface observations) to minimize the tropospheric contribution. More details on the determination of the respective contributions to the NO_2 absorption in the Fraunhofer reference spectrum are given in Sect. 3.1.3. Also a low order polynomial (representing the slow variation contribution of broad-band absorption, as well as the Rayleigh- and Mie-scattering processes) and a Ring spectrum (calculated by WinDOAS) are included. The cross sections of NO_2 (Burrows et al., 1998), O_3 (Burrows et al., 1999a), O_4 (Greenblatt et al., 1990), and H_2O from HITRAN (Rothman, 1998) are taken into account. The cross sections for NO_2 and O_3 at 223 K and 293 K are used (and the cross sections at cold temperature are orthogonalized with respect to those at high temperature) to account for the partitioning between the (warm) troposphere and (cold) stratosphere of these two trace gases. Thus the NO_2 fit results are a good approximation for the NO_2 absorptions at the high temperature. It should be noted that even in cases where this approximation is not well fulfilled, the effects on the tropospheric results are negligible because our technique includes the subtraction of the stratospheric NO_2 SCD from the measured total column (step 2 as described in Sect. 3.1). As result of the DOAS analysis, the differential slant column densities (DSCDs) of NO_2 were retrieved, which are the differences between the NO_2 slant column densities (SCDs, the integrated trace gas concentrations along the absorption path) of the measured spectra and the Fraunhofer reference spectrum.

2.2 Long-path DOAS measurements

In order to get the information about the NO_2 surface concentrations, a long-path DOAS instrument was installed at the same location as the zenith-sky instrument. Detailed description of the instrument can be found in Yu et al. (2004). In short, the collimated beam of white light from a 150 W Xe short-arc lamp is transmitted by a co-axial telescope to the open atmosphere and folded back into the telescope by an array of quartz corner cube retroreflectors, which was mounted at a distance of 507 m east of the experimental building and the same altitude as the telescope. Led by a quartz fiber, the light enters a spectrometer. Spectra in a wavelength range of 372–444 nm are recorded by a Czerny-Turner spectrograph with a focal length of 0.3 m, and detected by a 1024-pixel photodiode array detector cooled to $-15°$ C. With a fixed number of 20 scans (with an individual exposure time from 5 to 30 s), the average time resolution is about 4 min, which is similar to that of the zenith-sky measurements. The average NO_2 concentrations along the optical path are analyzed using the DOASIS software package (Kraus, 2001) in the spectral region of 424–435 nm, with the cross sections of NO_2 (Burrows et al., 1998) and O_3 (Burrows et al., 1999a) at 293 K, as well as the "background Fraunhofer structure" induced by the scattered sunlight received by the telescope (Zhou et al., 2005) taken into account. The retrieved amounts are taken as the NO_2 surface concentrations ($C_{surface}$) at the experimental site.

3 Deduction of the tropospheric NO_2 VCDs from ground-based instruments

3.1 Tropospheric NO_2 VCDs derived from zenith-sky observations

As mentioned in Sect. 2.1.2, the differential slant column densities (DSCDs) of NO_2 retrieved from zenith-sky measurements are the differences between total NO_2 columns contained in the measured and Fraunhofer reference spectra. In order to extract the tropospheric NO_2 vertical column densities (VCDs), there are three steps that should be followed:

(1) The NO_2 SCD in the Fraunhofer reference spectrum (SCD_{ref}) is added to the retrieved DSCDs to derive the total SCDs in the measured spectra (SCD_{meas});

(2) The stratospheric NO_2 SCDs (SCD_{strato}) are subtracted from the total ones to get the tropospheric NO_2 SCDs (SCD_{tropo});

(3) The tropospheric NO_2 SCDs (SCD_{tropo}) are divided by corresponding tropospheric air mass factors (AMFs) to get the tropospheric NO_2 VCDs (VCD_{tropo_zenith}) from zenith-sky measurements.

The strategy can be described by Eqs. (1–3) as below:

$$SCD_{meas} = DSCD + SCD_{ref} \quad (1)$$

$$SCD_{tropo} = SCD_{meas} - SCD_{strato} \quad (2)$$

$$VCD_{tropo\_zenith} = SCD_{tropo} / AMF_{tropo} \quad (3)$$

To perform these steps, several parameters have to be determined, including the tropospheric and stratospheric NO_2 AMFs (AMF_{tropo} and AMF_{strato}), SCD_{ref} and SCD_{strato} as

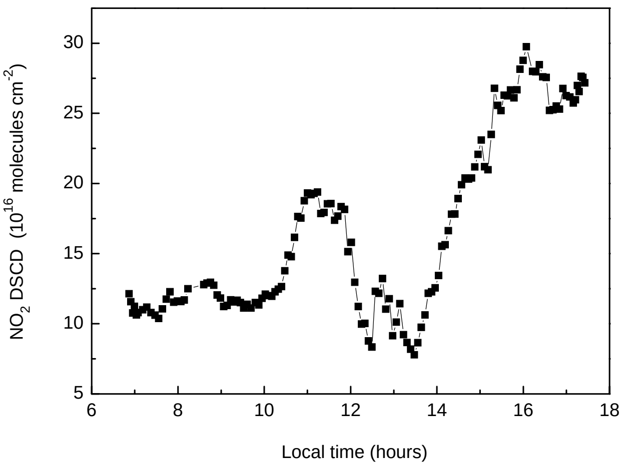

Fig. 1. Perturbation on zenith-sky measurements of NO_2 caused by strong tropospheric NO_x emissions (diurnal variation of the NO_2 DSCDs on 2 February 2007). Even during the twilight period, the measurements are dominated by the tropospheric NO_2 absorption.

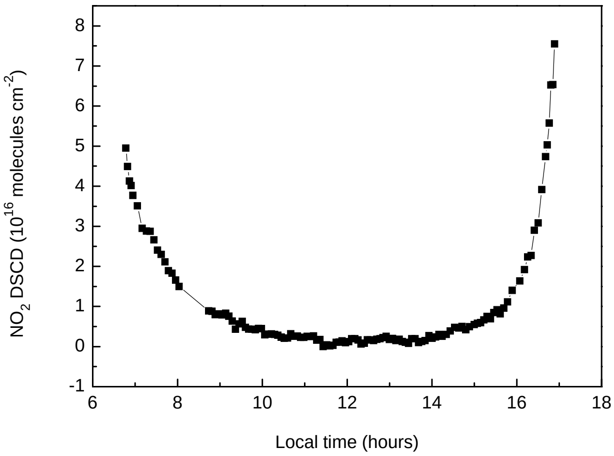

Fig. 2. Example of the diurnal variation of NO_2 DSCDs, which is dominated by the stratospheric absorption (observed at Chongming Island on 17 December 2006).

described in the following sections. For that purpose, some assumptions are made; the NO_2 surface concentrations acquired by long-path DOAS measurements are also used (for the selection of rather unpolluted days and for the determination of NO_2 absorption in the Fraunhofer reference spectrum).

3.1.1 Separation of the stratospheric NO_2 column densities

For practical reasons, here we do not strictly follow the order described above (Eqs. 1 to 3). Instead, step 1 will be described in Sect. 3.1.3, because it makes use of quantities defined in the current section. The observation of stratospheric NO_2 columns is possible during the twilight period, in which the sensitivity of zenith-sky instruments is greatly enhanced as the result of a long light path in stratosphere but a short path in troposphere. When the sun is low, the stratospheric AMF is much larger than the tropospheric one, which is always close to unity except in the presence of tropospheric clouds (e.g. Wagner et al., 1998; Pfeilsticker et al., 1998). Therefore, our first idea was to retrieve daily stratospheric NO_2 columns from sunrise and sunset spectra at SZAs near 90°. However, as Roozendael et al. (1994) pointed out, even during twilight period, the pollution episodes near the ground could significantly increase the measured total absorption and thus introduce large errors in the observations of stratospheric NO_2. Unfortunately, this is the case at the present urban site, which always suffers from heavy traffic pollution. The perturbation caused by tropospheric NO_2 to the twilight retrieval results is illustrated in Fig. 1, which shows the diurnal variation of NO_2 DSCDs on 2 February 2007 with a Fraunhofer reference spectrum measured at the noon of 26 February 2007 (clear day). The non-U-shape variation of the NO_2 DSCDs indicates a strong interference of tropospheric NO_2 pollution. Because such influence is always large in the urban site, the twilight data fail to provide useful information about the stratospheric NO_2 columns.

Instead, the three-day zenith-sky observations at Chongming Island serve for this aim. Figure 2 shows the measured NO_2 DSCDs on 17 December 2006 with a Fraunhofer reference spectrum taken at local noon of the same day. The U-shape variation suggests a low or constant tropospheric NO_2 amount. Considering the meteorological condition of that day, including all-day sea wind with high speed and the observation of a clear sky with high visibility, the NO_2 concentration in the boundary layer must be very low. Therefore, we use these observations to estimate the stratospheric NO_2 SCDs. First, the stratospheric NO_2 VCDs (VCD_{strato}) are deduced from the twilight measurements with the equations below (following from Eq. 1):

$$\begin{aligned} \mathrm{DSCD} &= \mathrm{SCD_{meas}} - \mathrm{SCD_{ref}} \\ &= \mathrm{VCD_{strato}} * \mathrm{AMF_{meas}} - \mathrm{VCD_{strato}} * \mathrm{AMF_{ref}} \end{aligned} \quad (4)$$

$$\mathrm{VCD_{strato}} = \mathrm{DSCD} \big/ \mathrm{DAMF} \quad (5)$$

where SCD_{ref} and SCD_{meas} are the NO_2 SCDs in the Fraunhofer reference spectrum and that measured during twilight, respectively; while AMF_{ref} and AMF_{meas} are the corresponding stratospheric AMFs (see Sect. 3.1.2); DAMF is the difference between AMF_{meas} and AMF_{ref}. The diurnal variation of the stratospheric NO_2 VCDs was ignored for the determination of the VCD_{strato} during twilight according to Eqs. (4) and (5); however, the corresponding errors are only small (about 2%), because for large SZA, AMF_{meas} is typically much larger than AMF_{ref}. By averaging the VCD_{strato} between 88–90° SZAs, the a.m. and p.m. stratospheric NO_2 vertical column densities

Table 1. Seasonal aerosol scenarios for the simulation of tropospheric NO_2 AMFs. The asymmetry parameter (0.68) and single scattering albedo (0.95) were assumed to be constant for all seasons.

Season	Aerosol optical depth (AOD)	Altitude range/ PBL height (km)
Winter (December, January and February)	0.6	0–0.5
Spring (March, April and May)	1	0–0.8
Summer (June, July and August)	1.2	0–1
Autumn (September, October and November)	0.8	0–0.8

were derived, which are 2.9×10^{15} molecules cm^{-2} and 4.0×10^{15} molecules cm^{-2}, respectively.

According to Lambert et al. (2002), the typical NO_2 cycle in the daytime displays a quasi-linear slow increase due to the NO_2/NO photochemical equilibrium and photolysis of N_2O_5. Therefore, the diurnal NO_2 stratospheric VCDs can be estimated by making a linear interpolation between the a.m. and p.m. VCD_{strato} over the whole day. Finally, by multiplying VCD_{strato} by the corresponding stratospheric AMF, the SCD_{strato} was derived. These SCD_{strato} were then used in Eq. (2).

The SCD_{strato} calculated in this way were taken as the typical stratospheric columns in Shanghai from 22 December 2006 to 31 March 2007, and used to deduce the tropospheric VCDs from observations at the urban site. The underlying assumption of spatial and temporal invariance of stratospheric NO_2 is certainly an error source in the extraction process. However, for polluted areas, the uncertainty caused by the stratospheric part should be rather small (especially for small SZAs). In order to reduce this error, another two pairs of a.m. and p.m. stratospheric values (3.7×10^{15} molecules cm^{-2} and 5.9×10^{15} molecules cm^{-2}, 2.6×10^{15} molecules cm^{-2} and 5.6×10^{15} molecules cm^{-2}, respectively) measured at the urban site during twilight periods on 22 May 2007 and 17 September 2007 were chosen to process data from April to July and August to December 2007, respectively. These two days are also characterized by ideal meteorological conditions and low surface NO_2 concentrations (demonstrated by the results of long-path DOAS measurements).

3.1.2 Calculation of the stratospheric and tropospheric AMFs

The stratospheric and tropospheric NO_2 AMFs used in this study for SCD to VCD conversion were calculated at 448 nm with the radiative transfer model TRACY-II (Deutschmann and Wagner, 2006; Wagner et al., 2007), in which the radiative transfer equation (RTE) is solved in a spherical three dimensional slice of the atmosphere, using the backward Monte Carlo formalism. Clouds and aerosol above 2 km are not included in the simulation. The surface albedo is set to 0.18. The monthly and latitudinal-averaged vertical profiles for pressure, temperature and ozone at 30° N–40° N are taken from the McLinden climatology contained in SCIATRAN database (Institute of Remote Sensing University of Bremen, 2004). In the AMF calculation, the NO_2 vertical profile is a key parameter affecting the results. For the stratospheric AMFs, the NO_2 profiles in McLinden climatology are used with no NO_2 below 2 km. While for the tropospheric AMFs, the assumed seasonal NO_2 profiles representing winter (December, January and February), spring (March, April and May), summer (June, July and August) and autumn (September, October and November) respectively are adopted with constant tropospheric NO_2 concentration (5.4×10^{11} molecules cm^{-3}, equal to 20 ppb at the ground level) within the PBL, which extends to different altitudes according to the seasons. It should be noted that the assumed profiles can only be seen as a rough estimate. Accurate information on the PBL height is difficult to obtain and the selected values should at least reflect the correct range of height variations. But fortunately, the tropospheric AMF does only weakly depend on these assumptions (see Sect. 3.1.5). Aerosol is assumed to be located at the same altitude range as the tropospheric NO_2, with the uniform asymmetry parameter (0.68) and single scattering albedo (SSA, 0.95) for all seasons. According to Duan and Mao (2007), the maximum atmospheric aerosol optical depth (AOD) over the Yangtze River Delta occurred in summer, followed by spring, autumn and the minimum value in winter. Therefore, we adopted the similar seasonal aerosol scenarios in TRACY-II (see Table 1) and modeled the corresponding seasonal tropospheric NO_2 AMFs, as shown in Fig. 3.

However, it is important to note that due to the changes of meteorological and pollution conditions, in reality the PBL height and AOD do not remain constant, neither does the tropospheric AMF. The uncertainties caused by the tropospheric NO_2 profiles, aerosol settings, as well as the PBL height are discussed in Sect. 3.1.5.

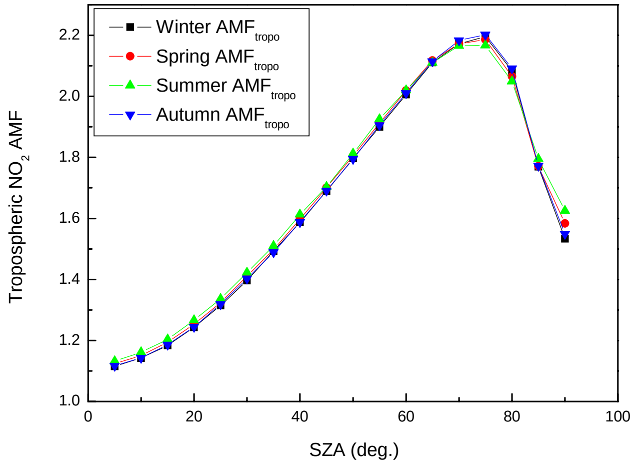

Fig. 3. Tropospheric NO_2 AMFs modeled by the radiative transfer model TRACY-II assuming seasonal NO_2 profiles and aerosol scenarios.

3.1.3 Determination of NO_2 SCDs in the Fraunhofer reference spectra

The SCDs in the Fraunhofer reference spectra can be divided into the stratospheric and tropospheric parts.

$$\mathrm{SCD_{ref}} = \mathrm{SCD_{strato\_ref}} + \mathrm{SCD_{tropo\_ref}} \quad (6)$$

The derivation of the former had been described in Sect. 3.1.1. The latter is determined by the equation below:

$$\mathrm{SCD_{tropo\_ref}} = \mathrm{VCD_{tropo\_ref}} * \mathrm{AMF_{tropo\_ref}} \quad (7)$$

The calculation of tropospheric VCDs in the Fraunhofer reference spectra ($\mathrm{VCD_{tropo\_ref}}$) is performed using the surface concentrations measured by the long-path DOAS experiment. From the assumed NO_2 profiles (as described in Sect. 3.1.2), the corresponding tropospheric VCDs can be calculated by multiplying the NO_2 concentrations at the bottom of the profiles by the height of PBL. Following this method, the tropospheric VCD in the Fraunhofer reference spectrum was derived by using the average NO_2 concentration observed by the long-path DOAS measurements.

Here, the average of 5 surface concentration data measured around the time when the Fraunhofer reference spectrum was recorded was multiplied by the assumed seasonal PBL heights to deduce the tropospheric NO_2 VCD in the Fraunhofer reference spectrum. The $\mathrm{SCD_{ref}}$ (e.g. in the Fraunhofer reference spectrum measured at noon on 26 February 2007) was determined to $(8.0\pm1.0)\times10^{15}$ molecules cm^{-2}. The $\mathrm{SCD_{strato\_ref}}$ and $\mathrm{SCD_{tropo\_ref}}$ were $(4.5\pm0.5)\times10^{15}$ molecules cm^{-2} and $(3.5\pm0.5)\times10^{15}$ molecules cm^{-2}, respectively. It should be noted that a single Fraunhofer reference spectrum was used for the analysis of a large period of time. Thus the potential errors in the determination of $\mathrm{SCD_{ref}}$ would affect all observations in a similar way. Thus, in particular the relative variation of the derived tropospheric VCDs does hardly depend on the determined absolute value of $\mathrm{SCD_{ref}}$.

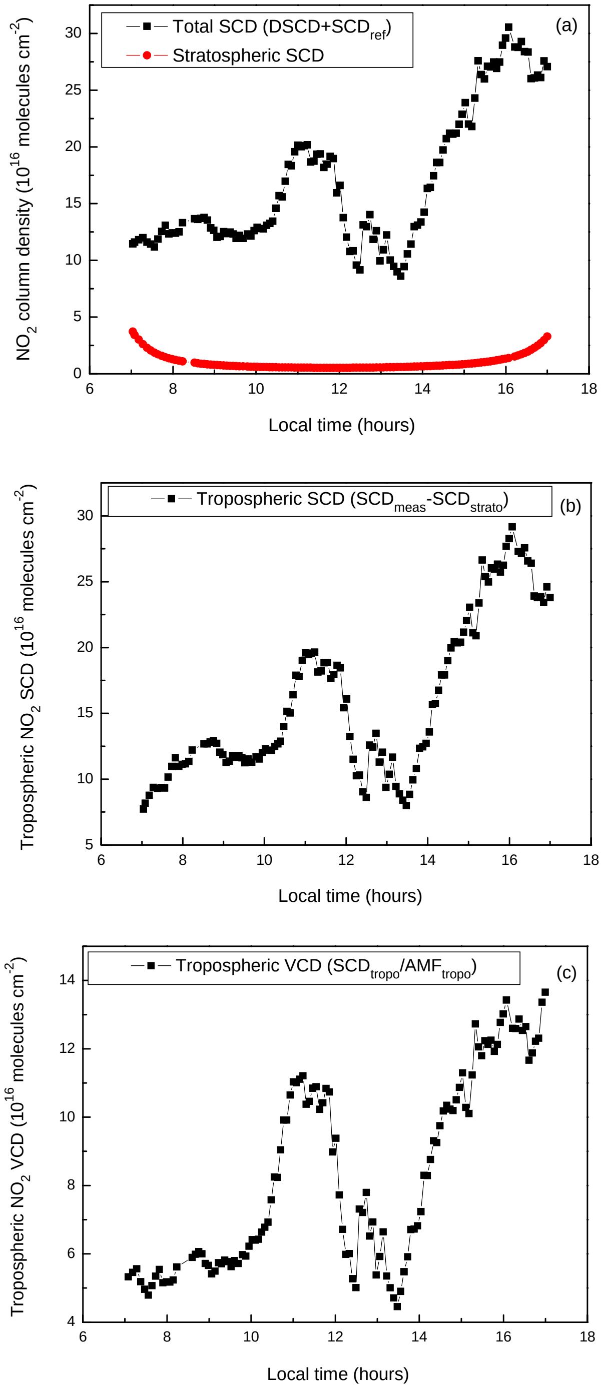

Fig. 4. Extraction of the tropospheric NO_2 VCD from zenith-sky observations. **(a)** Diurnal variation of the total NO_2 SCD and the deduced stratospheric SCD on 2 February 2007; **(b)** tropospheric NO_2 SCDs; **(c)** tropospheric NO_2 VCDs.

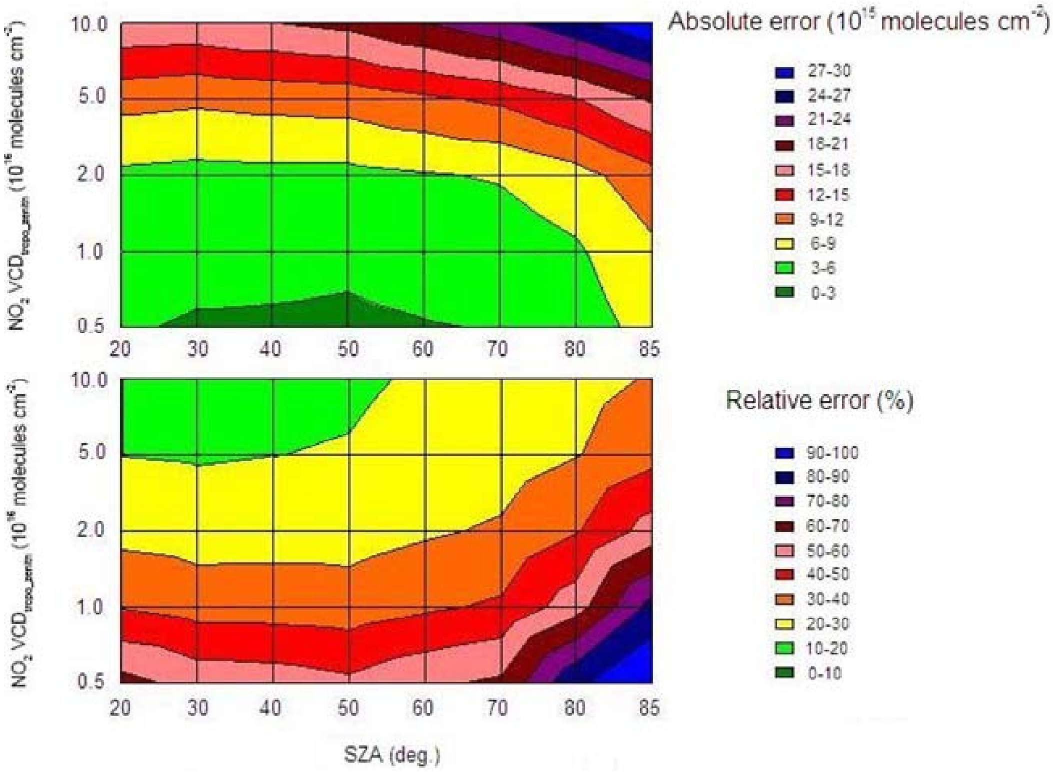

Fig. 5. Dependence of the absolute (top) and relative (bottom) errors of the tropospheric NO_2 VCDs on the SZA and the tropospheric NO_2 VCD. The different error contributions are added; thus the real errors might be typically smaller since the contributing errors will partly cancel each other.

With the above parameters, the tropospheric NO_2 vertical columns were finally extracted from the zenith-sky observations. Figure 4 shows the deduction process of the diurnal VCD_{tropo_zenith} on 2 February 2007, including the variation of the total SCDs (SCD_{meas}), the stratospheric SCDs (SCD_{strato}) (Fig. 4a), the tropospheric SCDs (SCD_{tropo}) (Fig. 4b) and the deduced tropospheric VCDs (VCD_{tropo_zenith}) (Fig. 4c). Comparing Fig. 4c with Fig. 4a, we can find that the tropospheric VCDs and total SCDs display the same variation, which indicates the dominance of the tropospheric part in the total column, as well as a severe pollution in the lower atmosphere.

3.1.4 Error estimation

There are several error sources contributing in a different way to the total error $\Delta VCD_{tropo\_zenith}$ of the tropospheric NO_2 VCDs (VCD_{tropo_zenith}). They can be divided into three categories E_1, E_2, and E_3, which affect $\Delta VCD_{tropo\_zenith}$ in different ways:

$$\begin{aligned} &\Delta VCD_{tropo\_zenith} \\ &= E_1 * VCD_{tropo\_zenith} + E_2\,(SZA) \\ &+ E_3\,(SZA) * VCD_{tropo\_zenith} \end{aligned} \tag{8}$$

E_1 describes uncertainties which directly scale with VCD_{tropo_zenith}. These errors are caused by the uncertainty of NO_2 absorption cross section and its temperature dependence. We estimate these uncertainties to 10% (Vandaele et al., 1998; Burrows et al., 1998). In this study we don't correct for the changing near surface temperature during the measurement period. Thus, the values during winter are systematically overestimated (e.g. by about 8% for a temperature of 273K). In future applications, a correction of the temperature effect should be applied. However, here we are mainly interested in the comparison of the different data sets which are affected by the temperature dependence of the NO_2 cross section in a similar way.

E_2 describes uncertainties which do not depend on the VCD_{tropo_zenith}. They arise from several sources:

(a) The error from the spectral retrieval. It is estimated from the magnitude of the residual structures of the DOAS analysis to about 5×10^{14} molecules cm^{-2}.

(b) The error from the determination of SCD in the Fraunhofer reference spectrum. It is estimated to about 1×10^{15} molecules cm^{-2} from the NO_2 concentrations observed by the long-path DOAS instruments during the time of measurement of the Fraunhofer reference spectrum.

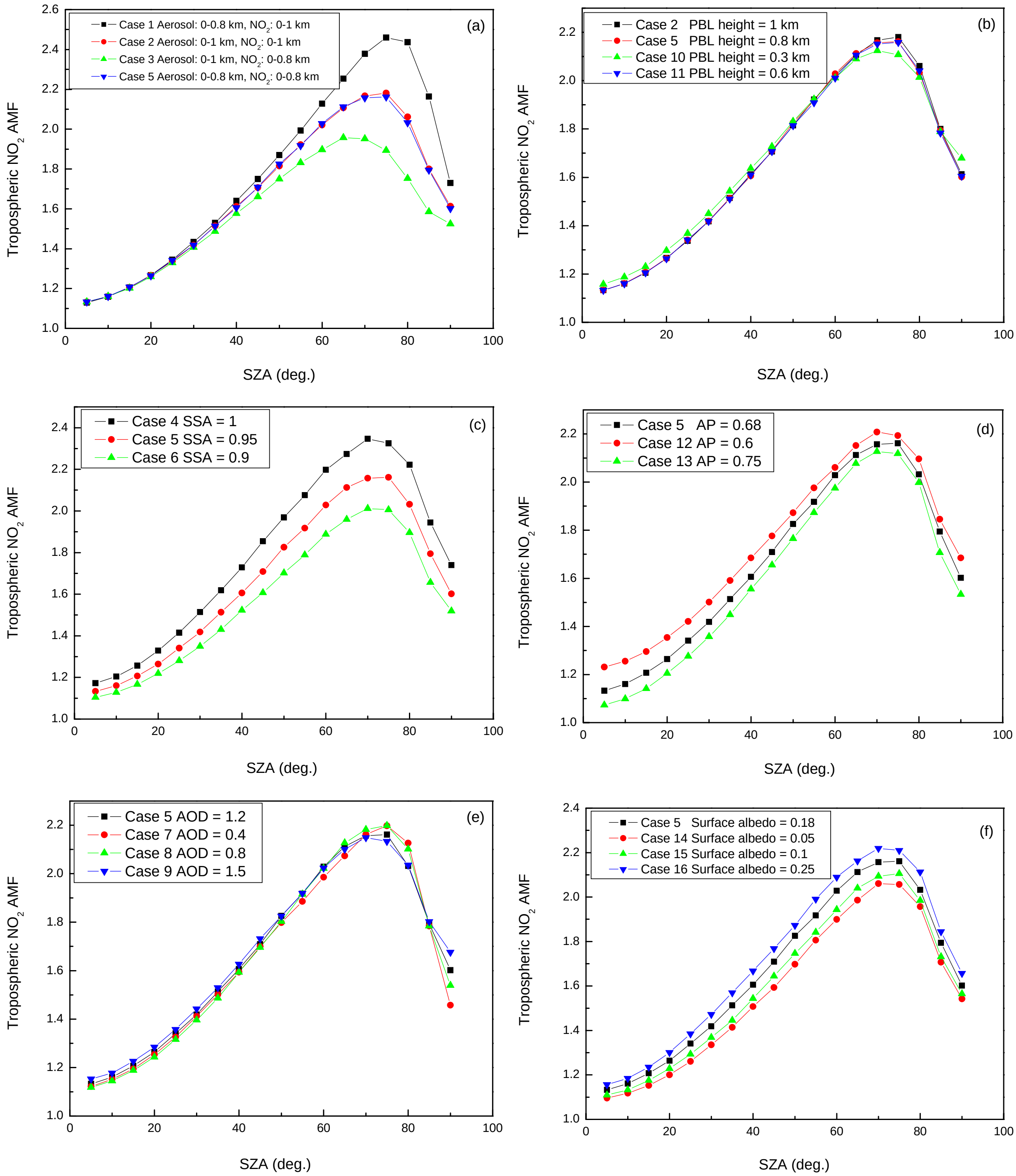

Fig. 6. Case studies of the influence of aerosol settings, profile assumptions, and surface albedo on the tropospheric NO_2 AMFs, modeled with the radiative transfer model TRACY-II. The tropospheric NO_2 AMFs deduced under the assumption **(a)** that the aerosol layer extends lower or higher than the tropospheric NO_2, **(b)** of different PBL heights, **(c)** of different aerosol single scattering albedos (SSA), **(d)** of different asymmetry parameters (AP), **(e)** of different aerosol optical depths (AOD), and **(f)** of different surface albedos. The detailed parameter settings of each case can be found in Table 2.

Table 2. Tropospheric NO_2 and aerosol settings for different test cases.

Case	The extension of aerosol layer (km)	The extension of tropospheric NO_2 layer (km)	Aerosol single scattering albedo	Surface Albedo	AP	AOD
1	0–0.8	0–1	0.95	0.18	0.68	1.2
2	0–1	0–1	0.95	0.18	0.68	1.2
3	0–1	0–0.8	0.95	0.18	0.68	1.2
4	0–0.8	0–0.8	1	0.18	0.68	1.2
5	0–0.8	0–0.8	0.95	0.18	0.68	1.2
6	0–0.8	0–0.8	0.9	0.18	0.68	1.2
7	0–0.8	0–0.8	0.95	0.18	0.68	0.4
8	0–0.8	0–0.8	0.95	0.18	0.68	0.8
9	0–0.8	0–0.8	0.95	0.18	0.68	1.5
10	0–0.3	0–0.3	0.95	0.18	0.68	1.2
11	0–0.6	0–0.6	0.95	0.18	0.68	1.2
12	0–0.8	0–0.8	0.95	0.18	0.6	1.2
13	0–0.8	0–0.8	0.95	0.18	0.75	1.2
14	0–0.8	0–0.8	0.95	0.05	0.68	1.2
15	0–0.8	0–0.8	0.95	0.1	0.68	1.2
16	0–0.8	0–0.8	0.95	0.25	0.68	1.2

(c) The error from the determination of stratospheric SCDs, which typically constitutes the largest contribution to E_2. This contribution is estimated from the variation of the stratospheric NO_2 VCDs over Shanghai as observed in SCIAMACHY limb observations, which are only sensitive to the stratospheric part of the total column (Kühl et al., 2008; Puķīte et al., 2008). Part of the seasonal variation of the stratospheric VCDs over Shanghai is accounted for by selecting different reference values for different seasons (see Sect. 3.1.1). The remaining variation of the stratospheric VCDs as estimated from the SCIAMACHY limb observations is up to about 1×10^{15} molecules cm^{-2}. Taking into account also the uncertainty of the stratospheric AMFs, the total uncertainties of the stratospheric SCDs result in values between 1.1×10^{15} molecules cm^{-2} (for SZA of 20°) and 1×10^{16} molecules cm^{-2} (for SZA of 85°).

E_3 describes the errors which scale with VCD_{tropo_zenith}, but depend also on other effects, mainly the SZA. A large fraction of these errors is caused by the uncertainties of the tropospheric AMFs. From detailed sensitivity studies using various input parameters for the radiative transfer simulations (see Sect. 3.1.5), these uncertainties are estimated to range between 10% and 20% for SZA of 20° and 85°, respectively.

The total error calculated according to Eq. (7) as function of the solar zenith angle and the total tropospheric VCD is shown in Fig. 5. In general, for small tropospheric VCDs, the largest contribution is caused by the uncertainties of the estimation of stratospheric SCDs, whereas for large tropospheric VCDs, the uncertainties in the determination of tropospheric AMFs dominate. The largest absolute errors occur for large SZAs and large VCD_{tropo_zenith}. The largest relative errors occur for large SZAs and small VCD_{tropo_zenith}. For a VCD_{tropo_zenith} of 5×10^{16} molecules cm^{-2} the relative error is <25% for SZA<70°. It should be noted that this error estimate is rather conservative, since the individual contributions in Eq. (7) are simply added. In reality, the different contributions, however, will partly cancel each other.

3.1.5 The influence of aerosol settings and profile assumptions on the tropospheric AMF

The sets of tropospheric NO_2 AMFs shown in Fig. 3 are based on aerosol and profile properties reflecting their seasonal variations. One important assumption is that the tropospheric NO_2 and aerosol layers are located within the same altitude range. This assumption is the most feasible one we can make here (the possible location and extension of tropospheric NO_2 and aerosol layers are too variable to be

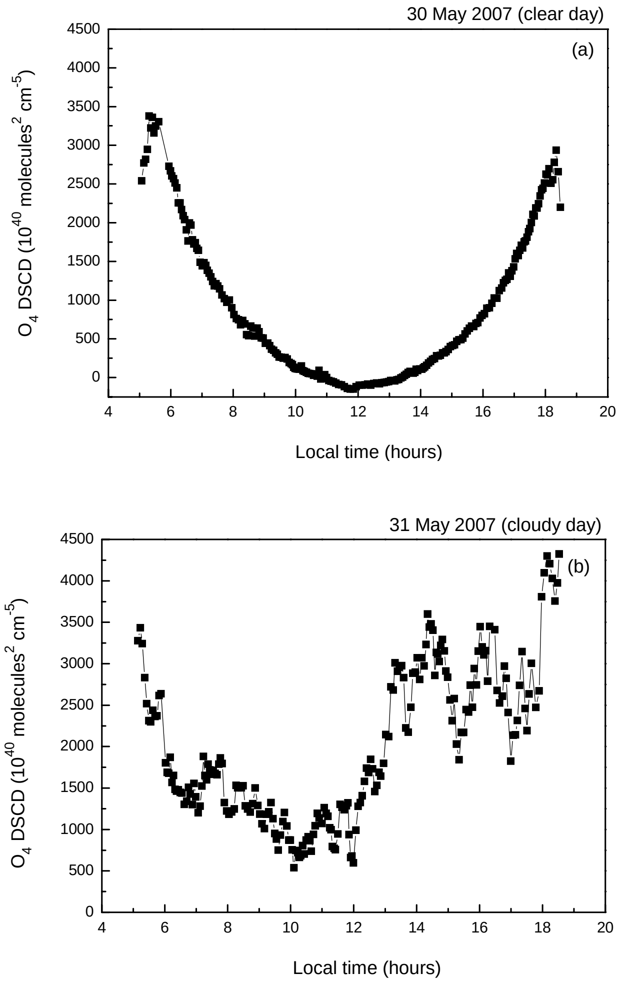

Fig. 7. Diurnal variations of the O_4 DSCDs on a clear (30 May 2007, **a**) and a cloudy day (31 May 2007, **b**), respectively.

comprehensively included in this study). Also the single scattering albedo and asymmetry parameter are fixed to values of 0.95 and 0.68, respectively. However, still rather large uncertainties exist about the aerosol properties as well as on the individual altitude profiles of the aerosol properties and NO_2 concentrations. In this section, we investigate these uncertainties by varying the different input parameters for the radiative transfer simulations. As reference case, the tropospheric NO_2 AMFs simulated for a layer height (aerosol and NO_2) of 0.8 km, aerosol optical depth of 1.2, single scattering albedo of 0.95, asymmetry parameter of 0.68 and surface albedo of 0.18 are selected (case 5 in Table 2).

First, we investigate the effect of the relative location of the tropospheric NO_2 and the aerosol layers on the tropospheric AMFs by extending them to different altitudes (cases 1–3, 5 in Table 2). Figure 6a shows the tropospheric AMFs deduced under the assumptions that the aerosol layer extends lower (case 1) and higher (case 3) than the tropospheric NO_2, respectively. Because of the multiple scattering effect of aerosol, when the top of aerosol layer is located above the tropospheric NO_2, a greater fraction of the observed photons passes the NO_2 layer on a vertical rather than on a slant path (depending on the SZA). Thus, the deduced tropospheric AMFs are reduced, especially for SZA larger than 70°. Similarly, the tropospheric AMFs can be enhanced if the top of the aerosol layer falls below that of the tropospheric NO_2. It should be noted that since the dominant fraction of VCD_{tropo_zenith} was observed at small SZAs, the differences become rather small. Thus potential variations of the relative locations of tropospheric NO_2 and aerosol layers would not cause large error to the results.

Secondly, in order to investigate the influence of the layer height itself, we assume that the layers of both the tropospheric NO_2 and the aerosol simultaneously extend to different altitudes (cases 2, 5, 10, 11 in Table 2). The results shown in Fig. 6b indicate that the layer height has only a very small influence on tropospheric AMFs.

Thirdly, the influence of aerosol single scattering albedo (SSA) on the derived tropospheric AMFs is tested (cases 4–6 in Table 2). It is found that (Fig. 6c) the tropospheric AMFs increase with increasing single scattering albedo. Since 0.95 is probably the most realistic value of aerosol single scattering albedo, the errors caused by an assumed uncertainty of the single scattering albedo in the range of 0.9 to 1 are below 10% for SZAs lower than 85°.

Fourthly, the influence of the aerosol asymmetry parameter (AP) is investigated (cases 5, 12, 13 in Table 2). As shown in Fig. 6d, especially for small SZAs, uncertainties of the asymmetry parameter can cause relatively large errors in the tropospheric AMFs (up to about 10%).

Fifthly, the effect of AOD settings on the tropospheric AMFs is investigated, with AOD assumed to be 0.4, 0.8, 1.2 and 1.5 (cases 5, 7–9 in Table 2). Like the layer height (Fig. 6b), also the aerosol optical depth has only a relatively small influence on the tropospheric AMFs (Fig. 6e).

Finally, we investigate the influence of the surface albedo (values from 5% to 25%) on the modeled tropospheric AMFs (cases 5, 14–16 in Table 2). It is demonstrated in Fig. 6f that the uncertainties of the surface albedo cause rather small errors in the tropospheric AMFs (up to about 5% for the assumed range of albedo values).

From the above discussions we conclude that though the respective uncertainties in several groups of cases are up to 10%, the errors caused by the uncertainties of aerosol properties, as well as the aerosol and NO_2 profile settings might partly cancel each other. In this study we estimate the total uncertainty of the tropospheric NO_2 AMF to range between 10% and 20% for SZA at 20° and 85°, respectively.

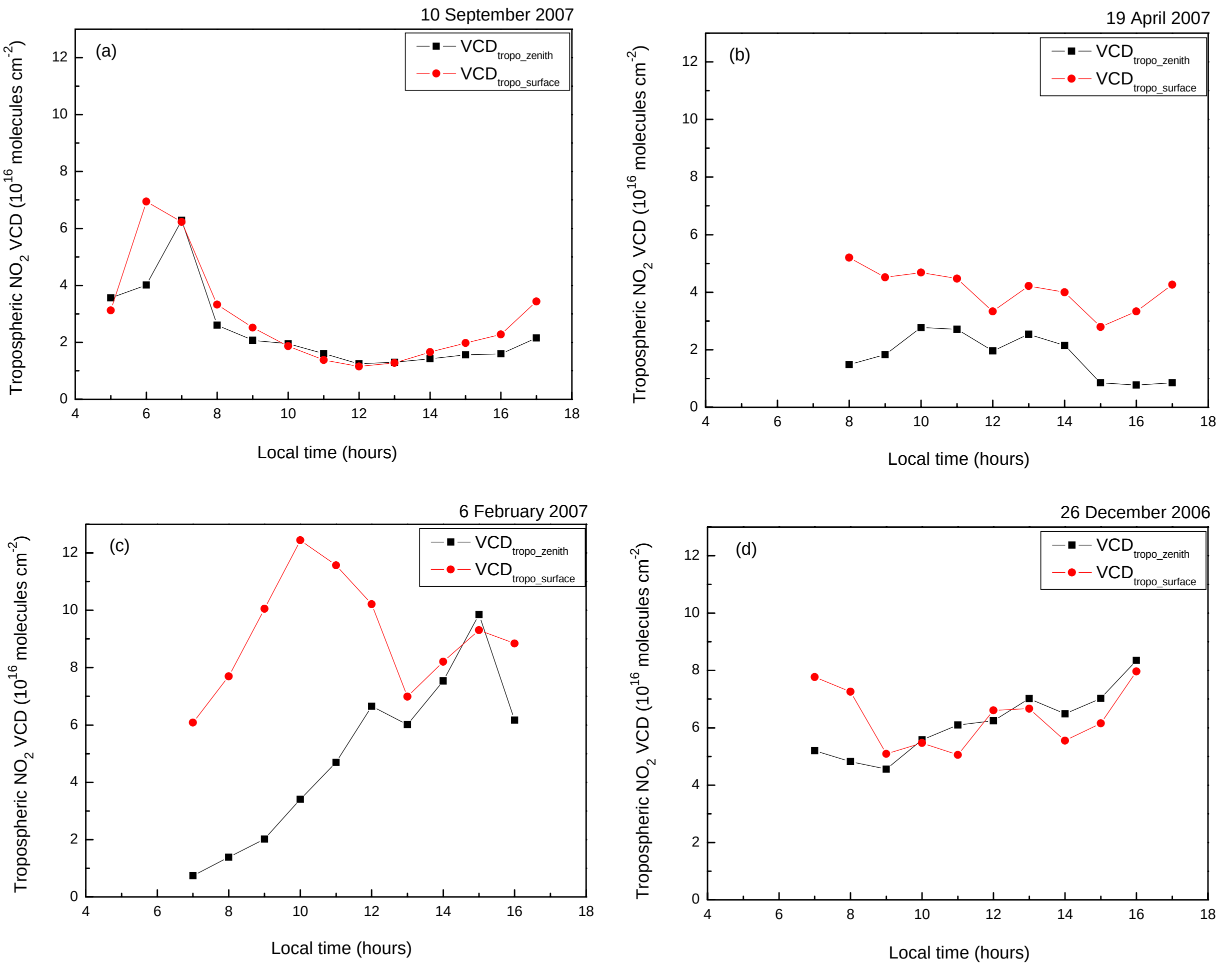

Fig. 8. Typical examples of comparisons between the tropospheric NO_2 VCDs from zenith-sky observations (VCD_{tropo_zenith}) and long-path DOAS observations ($VCD_{tropo\_surface}$).

3.2 Tropospheric NO_2 VCDs derived from long-path DOAS observations

In order to validate the extraction results, the hourly-averaged NO_2 surface concentrations measured by long-path DOAS observations are also converted into the corresponding tropospheric VCDs ($VCD_{tropo\_surface}$) by multiplying by the assumed seasonal PBL heights, and compared with the hourly-averaged VCD_{tropo_zenith}. It is interesting to note that, in contrast to the VCD_{tropo_zenith}, errors in the $VCD_{tropo\_surface}$ as a result of a wrong PBL height setting are directly proportional to the errors of the PBL height.

4 Results and discussion

In this section, the resulting tropospheric NO_2 VCDs derived from zenith-sky measurements are firstly compared with the VCDs converted from the surface concentrations. Then factors affecting the comparison are explored and discussed. Finally, a comparison between the tropospheric NO_2 VCDs derived from SCIAMACHY observations and ground-based measurements is presented.

4.1 Comparison between the tropospheric NO_2 VCDs deduced from zenith-sky and long-path DOAS measurements

Before the comparison, the potential influence of tropospheric clouds should be discussed. As demonstrated by Wagner et al. (1998) and Pfeilsticker et al. (1998), the photon diffusion in optical thick clouds and the multiple reflections between layers and patches of clouds can greatly enhance the light path. If there is NO_2 located at the cloud level, the absorption would become much larger than that under clear sky condition. On the other hand, in the presence of high thin clouds, the tropospheric absorption can also be slightly decreased. If in cloudy conditions, the tropospheric AMFs calculated under cloud-free assumption are used to retrieve

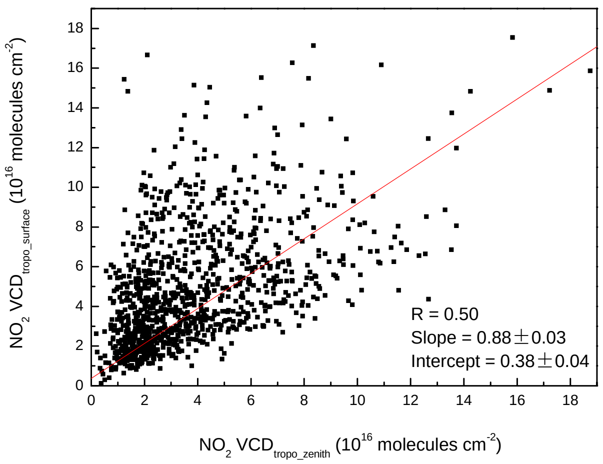

Fig. 9. Regression analysis of the tropospheric NO_2 VCDs derived from long-path DOAS observations ($VCD_{tropo\_surface}$) and zenith-sky observations (VCD_{tropo_zenith}) for 98 days under cloud-free condition.

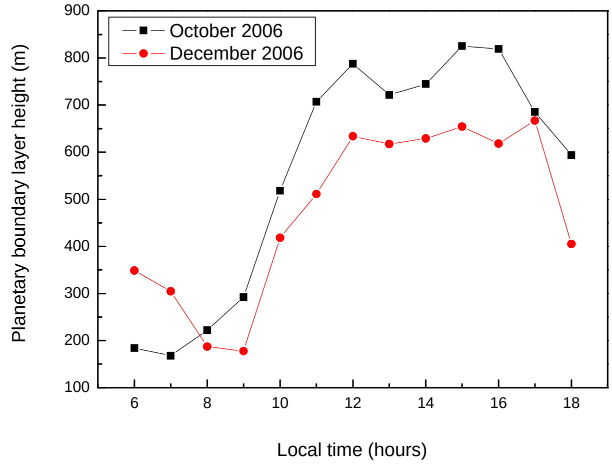

Fig. 10. Monthly-averaged diurnal Planetary Boundary Layer (PBL) height for Shanghai in October and December 2006, modeled and provided by Patrick Jöckel, modeling group at MPI for Chemistry, Mainz, Germany. The model results were taken from the S2 simulation of the Modular Earth Submodel System (MESSy), see Jöckel et al., 2006.

the tropospheric VCDs, large errors can occur. Without the information about the location and extension of clouds, as well as the distribution of NO_2 inside clouds, it is difficult to correctly extract the tropospheric NO_2 VCDs from zenith-sky measurements. Therefore, in this study, only the results for clear days are selected for comparison. Here the daily meteorological observations and the diurnal variation of the retrieved O_4 columns are combined to select days in which the cloud impact can be neglected. Because the O_4 concentration in the atmosphere mainly depends on the square of the O_2 concentration, and the atmospheric O_2 column varies only slightly (depending on pressure) (Perner and Platt, 1980; Greenblatt et al., 1990; Wagner et al., 2002; Wittrock et al., 2004), the O_4 absorption can be used as a criterion to identify the existence of clouds and aerosols. For a trace gas with constant amount in the atmosphere, the observed diurnal SCD variation shows a smooth increase with the increasing SZAs in clear sky condition (Meena et al., 2004). Therefore, here the U-shape diurnal variation of the retrieved O_4 DSCDs is taken as an indicator for a clear day. As shown in Fig. 7, using this criterion, it can be well distinguished between a clear day (30 May 2007) and a cloudy day (31 May 2007). Following the above criteria, data from 98 days under cloud-free conditions during 22 December 2006 to 31 December 2007 are chosen for comparison. The results are separated into four groups. Figure 8 shows typical examples for the selected days of each group. In the first group (including 12 days), both the hourly-averaged values and relative diurnal variations of the tropospheric NO_2 VCDs derived from zenith-sky observations (VCD_{tropo_zenith}) and long-path DOAS observations ($VCD_{tropo\_surface}$) present good agreements. In the second group (including 25 days), only the relative variations of VCD_{tropo_zenith} and $VCD_{tropo\_surface}$ agree. In the third group (including 33 days), VCD_{tropo_zenith} and $VCD_{tropo\_surface}$ have different values and relative variations. In the last group (including 28 days), the curves of diurnal VCD_{tropo_zenith} and $VCD_{tropo\_surface}$ intersect, but with different relative variations. As there are only one third of the days belonging to the first and second groups, the VCD_{tropo_zenith} and $VCD_{tropo\_surface}$ do not agree well.

The overall regression analysis of $VCD_{tropo\_surface}$ and VCD_{tropo_zenith} for cloud-free observations from 98 days is performed. Since there are uncertainties in both data sets, the standard least-squares method, which only minimizes the distances between the fitted line and the data in the y-direction, is not appropriate. Here a weighted bivariate least-squares method (Eqs. 5 and 6 in Cantrell, 2008), which considers the errors in both y- and x-variables, and minimizes the perpendicular distances between the fitted line and the data, is adopted. Such an algorithm allows assigning individual uncertainties to all data points. Therefore, an absolute plus a relative uncertainty of both measurements was estimated and applied to the regression. For VCD_{tropo_zenith}, the error is estimated to be 2×10^{15} molecules $cm^{-2}\pm20\%$; For $VCD_{tropo\_surface}$, the assumptions on the PBL height and on the homogenous mixing within the PBL are the dominant error sources. Thus, a relative error of about 40% is estimated (see also sections below). Using these assumptions, the fitted regression line, shown in Fig. 9, indicates a rather low correlation between the two data sets (R=0.50).

As mentioned in Sect. 3, the standardized seasonal shapes of NO_2 profiles were adopted to convert the surface concentrations into the tropospheric VCDs ($VCD_{tropo\_surface}$). However, due to the change of meteorological conditions

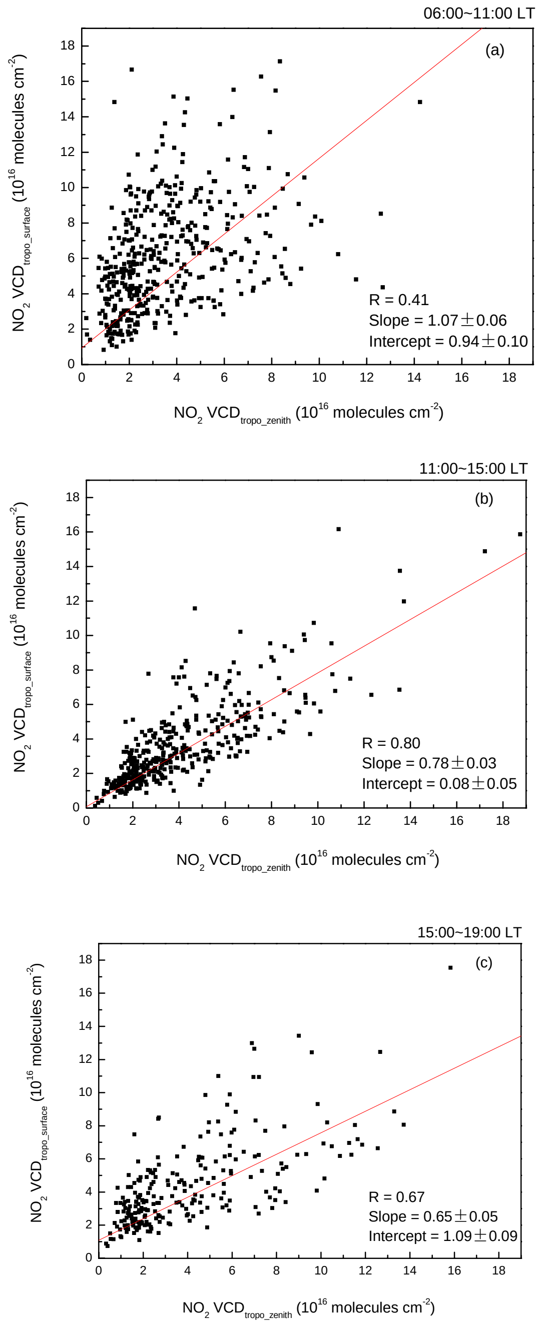

Fig. 11. Regression analysis of the tropospheric NO_2 VCDs derived from long-path DOAS observations ($VCD_{tropo\_surface}$) and zenith-sky observations (VCD_{tropo_zenith}) for three selected periods during the daytime (06:00∼11:00 LT, 11:00∼15:00 LT and 15:00∼19:00 LT).

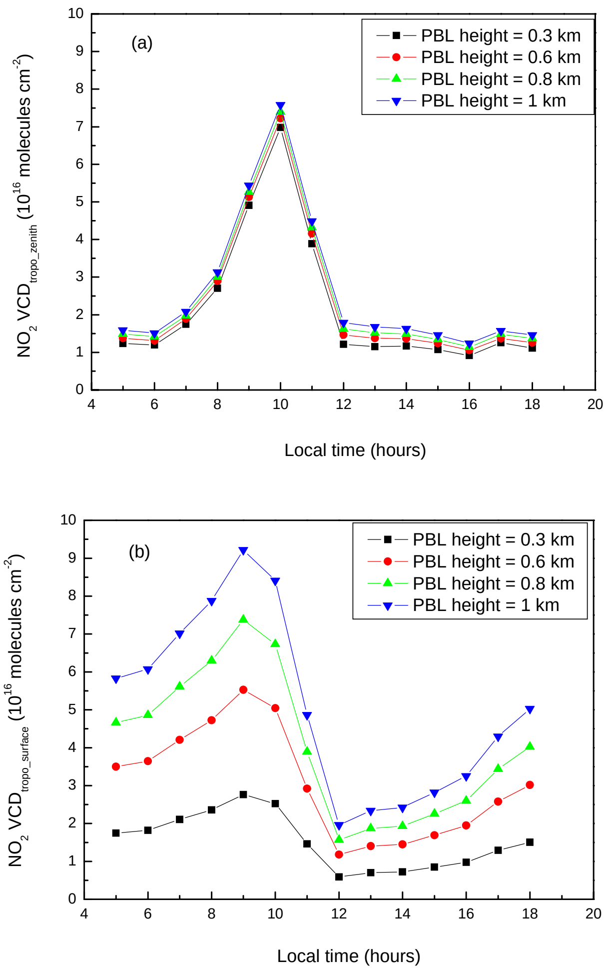

Fig. 12. (a) Corresponding tropospheric NO_2 VCDs from zenith-sky observations and **(b)** long-path DOAS observations for 9 June 2007, deduced under four PBL height assumptions.

during the day, the PBL height does not remain constant, especially in the situation of a temperature inversion. Daily comparison of $VCD_{tropo\_surface}$ and VCD_{tropo_zenith} always shows higher $VCD_{tropo\_surface}$ in the morning, which indicates an overestimation of the PBL height. Figure 10 shows the monthly-averaged diurnal PBL heights for Shanghai in October and December 2006, modeled and provided by Patrick Jöckel, modeling group at MPI for Chemistry, Mainz, Germany. The model results were taken from the S2 simulation of the Modular Earth Submodel System (MESSy, see Jöckel et al., 2006). The PBL height fluctuates sharply from 06:00 LT to 11:00 LT, and then remains relatively unchanged until 18:00 LT. In order to investigate the influence of the PBL height variation in more detail, the time from 06:00 LT to 19:00 LT is divided into 3 periods, which are 06:00∼11:00 LT, 11:00∼15:00 LT and 15:00∼19:00 LT, respectively. The orthogonal regression analysis of $VCD_{tropo\_surface}$ and VCD_{tropo_zenith} in each period (for all selected days) is shown in Fig. 11. As expected, the best correspondence happens in the second period, from 11:00 LT to 15:00 LT, in which the PBL height is more constant compared with the other two periods, and the influence of uncertainties caused by the stratospheric

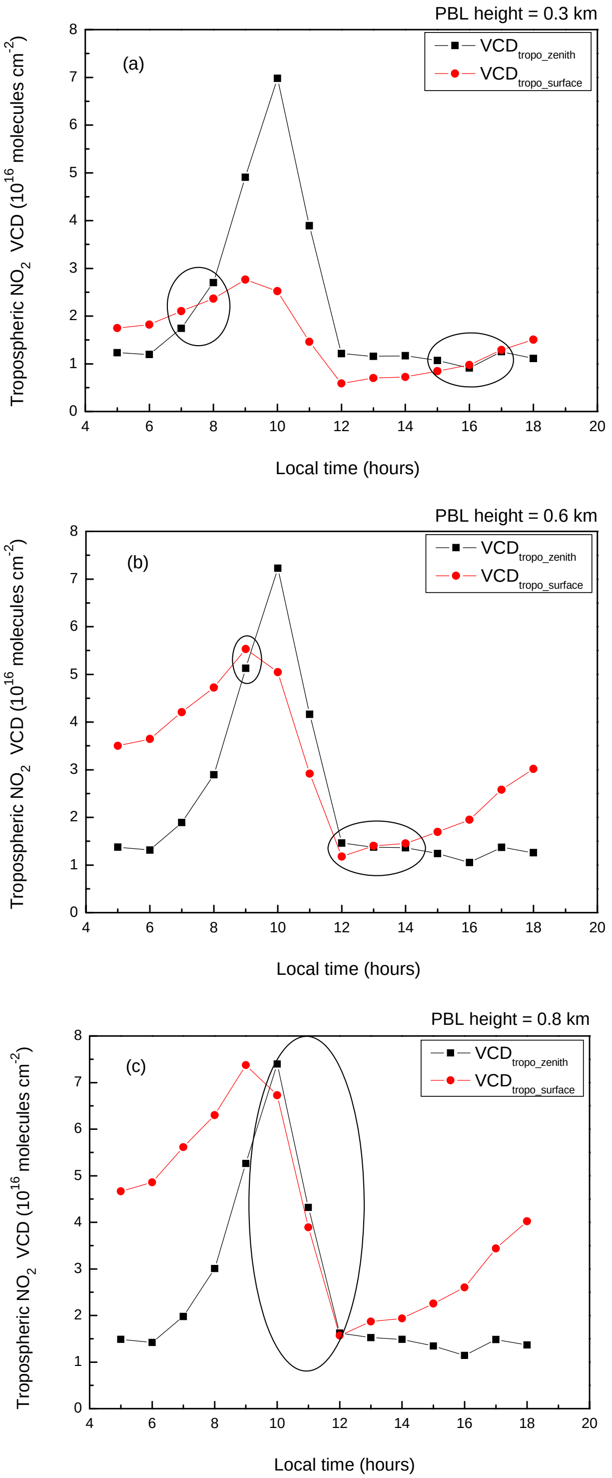

Fig. 13. Comparison between the tropospheric NO_2 VCDs derived from zenith-sky observations (VCD_{tropo_zenith}) and long-path DOAS observations ($VCD_{tropo\_surface}$) on 9 June 2007 under different PBL height assumptions. The circles indicate times when both data sets agree.

NO_2 VCD deduction is minimized because of the small SZAs. In addition, the correlation between $VCD_{tropo\_surface}$ and VCD_{tropo_zenith} in the third period is better than that in the first period, which further demonstrates the influence of PBL height variation on the comparison results.

It might be interesting to note that in Fig. 9 and Fig. 11, in general, a positive y-intercept is found. Although the values are rather small, this might indicate the influence of NO_2 in the free troposphere which will contribute to VCD_{tropo_zenith}, but not to $VCD_{tropo\_surface}$.

4.1.1 The influence of PBL height variations on the VCD_{tropo_zenith} and $VCD_{tropo\_surface}$ calculations

Figure 12a and b show the VCD_{tropo_zenith} and $VCD_{tropo\_surface}$ in 9 June 2007, deduced under the four PBL height assumptions defined in the previous section. The much larger deviations for the different profiles of $VCD_{tropo\_surface}$ than those for VCD_{tropo_zenith} demonstrate the big uncertainties of the conversion from surface concentrations to $VCD_{tropo\_surface}$. Thus one important conclusion of this comparison is that VCD_{tropo_zenith} is more reliable and probably more suitable for satellite validation. However, it should be pointed out that because the calculation of VCD_{tropo_ref} also involves the conversion of the NO_2 surface concentration into the tropospheric VCD using the PBL height information, it is important to choose a "clean" Fraunhofer reference spectrum, in which the NO_2 pollution in the lower atmosphere is small, to reduce the proportion of VCD_{tropo_ref} to the deduced VCD_{tropo_zenith}, and thus to enhance the reliability of VCD_{tropo_zenith}.

In addition, the comparison between VCD_{tropo_zenith} and $VCD_{tropo\_surface}$ deduced under the above different PBL height assumptions was made (see Fig. 13). The different extent of agreement in each group indicates the systematic variation of the PBL height during the course of the day (see also Fig. 10). Thus, from the comparison between VCD_{tropo_zenith} and $VCD_{tropo\_surface}$ on clear days, valuable information about the PBL height can be derived, which should be investigated in more detail in the future.

4.2 Comparison with SCIAMACHY tropospheric NO_2 VCDs

4.2.1 SCIAMACHY instrument and data analysis

SCIAMACHY (SCanning Imaging Absorption spectroMeter for Atmospheric CHartographY) is a 8 channel spectrometer aboard the European Space Agency's (ESA) Environmental Satellite (ENVISAT), and designed to measure the sunlight upwelling from the earth's atmosphere in different viewing geometries in the UV, visible and near infrared region (240–2380 nm) to retrieve the amounts and global distribution of various atmospheric trace gases (Bovensmann et al., 1999). Compared to GOME (Global Ozone Monitoring

Experiment), i.e. $40\times320\,km^2$, SCIAMACHY has a better spatial resolution of $30\times30\,km^2$ to $30\times240\,km^2$ (typically $30\times60\,km^2$), which is of great importance to accurately detect the enhanced NO_2 amount over some hot spots, which are always smoothed out in the GOME data (Beirle et al., 2004). Global coverage is achieved after every 6 days at the equator.

Details on the spectral analysis for GOME (adopted also to SCIAMACHY) can be found in Leue et al. (2001) and Beirle et al. (2003). The NO_2 columns are retrieved in the spectral window between 430–450 nm (channel 3). In order to separate the stratospheric NO_2 columns, the slant columns measured over the Pacific Ocean at the same latitude are taken as the stratospheric NO_2 background values, which were subtracted from the total slant columns to obtain the tropospheric NO_2 SCDs. Then, the tropospheric NO_2 VCDs are derived by dividing the tropospheric SCDs by the corresponding tropospheric AMFs (Richter and Burrows, 2002). Here, the AMFs are also calculated with the radiative transfer model TRACY-II for the following settings: for NO_2 a profile is assumed with 80% of the tropospheric column located between the surface and 1 km altitude (homogenous concentration) and the remaining 20% in the free troposphere from 1–15 km (constant mixing ratio); an aerosol layer of 1 km thickness, $0.5\,km^{-1}$ extinction, asymmetry parameter 0.68, and single scattering albedo 0.9 (all the aerosol optical parameters are for 440 nm) is assumed; the ground albedo is set to 5%. These setting are globally unique in our standard retrieval of tropospheric NO_2 columns. And it should be paid attention that though these standard settings for satellite retrieval are different from those used for the deduction from zenith-sky observations, as discussed in Sect. 3.1.5, the influence on the results of zenith scattered light observations is rather small (see also Fig. 6). AMFs according to these settings are first modeled separately for cloud free and clouded scenes for different cloud top heights (CTH). For the clouded scenes, simplified assumptions on the cloud properties are made (vertical extension of the cloud: 1 km, single scattering albedo: 1, asymmetry parameter: 0.85). In the second step, the actual AMFs for a given observation are calculated by weighting the AMFs for the clear and cloudy parts according to the effective cloud fraction (CF) given for the observations, and the modeled radiances of the clear and cloudy parts, respectively. The effective cloud fractions and cloud top heights are taken from the FRESCO (Fast Retrieval Scheme for Cloud Observables) algorithm (Koelemeijer et al., 2001, 2002). The errors of the tropospheric NO_2 VCD derived in this way are estimated to be 1×10^{15} molecules $cm^{-2}\pm30\%$, which are adopted in the orthogonal regression analysis below.

Here the additive part of the error (1×10^{15} molecules cm^{-2}) is caused by the stratospheric correction, which neglects longitudinal variations of stratospheric NO_2.

The multiplicative part of the error (30%) is caused by two sources:

(a) Temperature dependence of NO_2 cross section. The seasonal temperature changes can cause variations of NO_2 absorption of about 8%.

(b) Errors in the AMF calculation. These are dominated by uncertainties due to the assumed albedo of 5% (causing an uncertainty in tropospheric NO_2 VCDs of about 20%) and errors in the AMFs due to uncertain cloud properties (below 10% in most cases for an uncertainty of 0.02 (absolute) in cloud fraction).

It should be noted that, though the parameter settings for SCIAMACHY tropospheric AMF simulation do not completely agree with those used in ground-based tropospheric AMF simulation, which takes the seasonal variation into account, the differences would not cause large deviation to the deduced tropospheric VCDs, considering the magnitude of tropospheric AMFs in cloud free condition (close to 1). However, especially for clouded scenes and heavy aerosol loads, the choice of the tropospheric NO_2 profiles has a stronger impact on the satellite AMFs than for ground-based observations. The influence of the cloud properties on the comparison between ground-based and satellite data is investigated in more detail in Sect. 4.2.2.

The SCIAMACHY pixels used here are those covering the ground-based experimental site (31.3° N, 121.5° E). Considering the impact of clouds on the observations of trace gases below cloud top, we separated the data to those measured for cloud fractions higher or lower than 0.2 (cloudy and clear-sky conditions, respectively), and focus on the latter in the comparison with zenith-sky observations.

4.2.2 Comparison between tropospheric NO_2 VCDs from SCIAMACHY and ground-based measurements

For the comparison with the SCIAMACHY results, the one-hour average tropospheric NO_2 VCDs from the zenith-sky measurements during 10:00∼11:00 LT were used, which were observed around the time of SCIAMACHY overpass (SCIAMACHY's overpass over Shanghai for the coincidences is found about 10:20 LT). Here also tropospheric NO_2 VCDs from zenith-sky measurements, for partially clear days (with cloud free sky during the satellite overpass) were included in the comparison.

Figure 14a shows the orthogonal regression of the tropospheric NO_2 VCDs derived from SCIAMACHY and zenith-sky measurements under all cloud fractions in 2007 (data from 45 days), with a relative low correlation (black line, R=0.68). The separate regression analyses for data under clear-sky and cloudy conditions (red and blue, respectively, in Fig. 14a) are also performed, which show a better correlation for the former (R=0.75) but worse correlation for the latter (R=0.58).

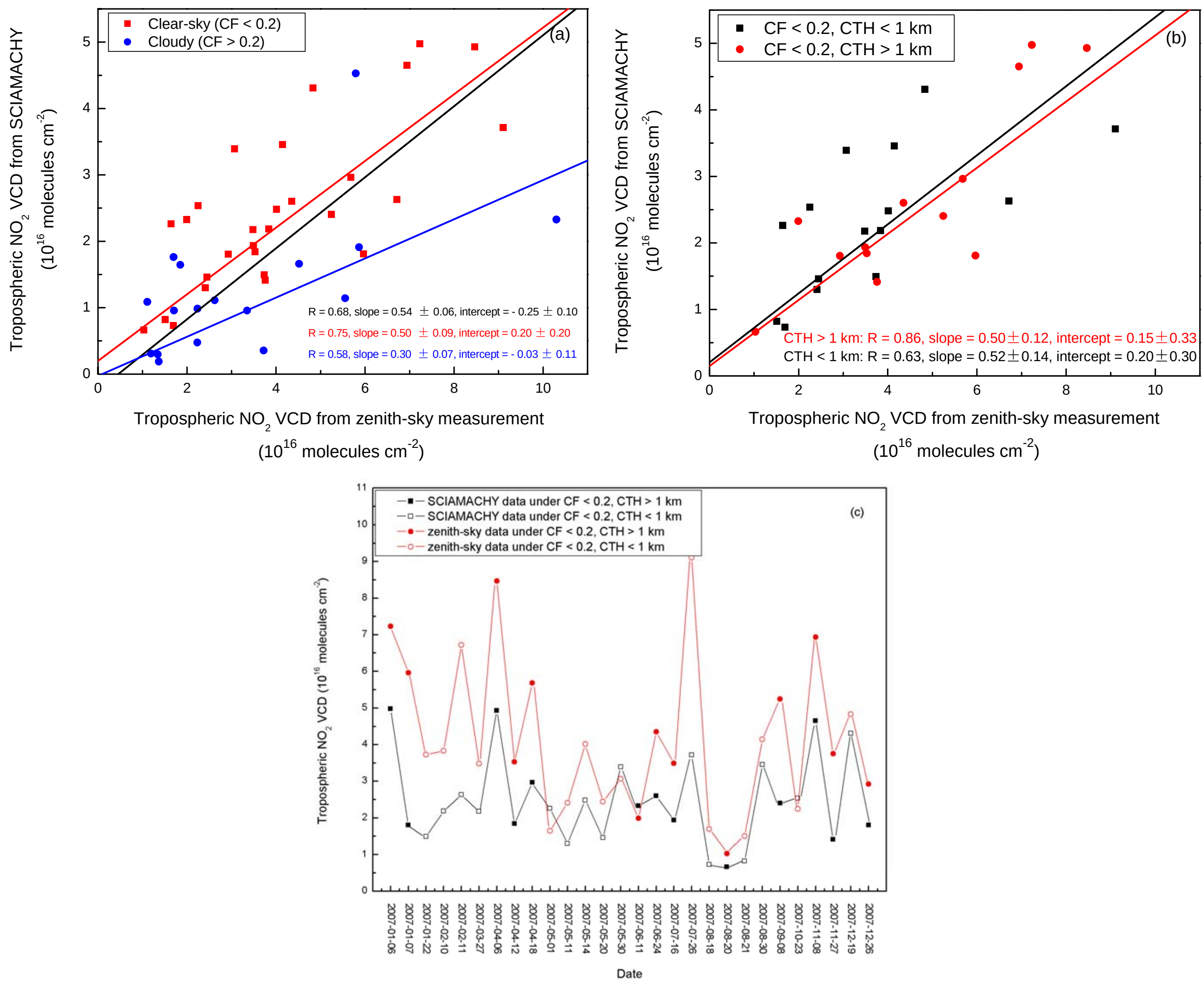

Fig. 14. Comparison between the tropospheric NO_2 VCDs deduced from SCIAMACHY and zenith-sky observations. **(a)** Orthogonal regression of the tropopheric NO_2 VCDs from SCIAMACHY and zenith-sky measurements under all cloud fractions (black fitted line). Red points represent the data for days under clear-sky condition, while the blue points represent the data for cloudy days; **(b)** Regression analysis of data for days with CF<0.2 & CTH<1 km (black points), and CF<0.2 & CTH>1 km (red points) respectively; **(c)** Comparison between the tropospheric NO_2 VCDs from SCIAMACHY and zenith-sky measurements under clear-sky condition (CF<0.2). Open squares and circles represent the satellite and zenith-sky data for days with CTH<1 km, respectively.

Since the correlation between the two measurements is not improved much when only the data under clear-sky condition are taken into account, we take a closer look at the corresponding days. It is found that there are more than half of the days (15 days) in which the FRESCO cloud top height (CTH) in the target SCIAMACHY pixels are below 1 km. These cases cannot be processed in the usual way of data retrieval, in which the model cloud is 1 km thick. Such observations are probably related to the presence of substantial aerosol loads; hence these scenes (as long as cloud fraction is below 0.2) are all treated as if they are cloud free with a homogenous aerosol layer. Depending on the actual scene, the true AMF could be high (due to the multiple scattering within a scattering aerosol layer, or low cloud in the polluted layer) or low (in case of absorbing aerosol or pollution located below the cloud). Therefore, the tropospheric NO_2 VCDs from SCIAMACHY (having AMF of about ∼1.2 for these scenes) could be over- or underestimated. Considering the uncertainties of the satellite data for days with CF<0.2 and CTH<1 km, we mark those data and analyze the correlation for the remaining clear-sky data (days with CF<0.2 and CTH>1 km). As shown in Fig. 14b, the correlation is greatly improved (R=0.86) when the days with CTH<1 km are excluded. It should be noted that because of the small number

Table 3. Comparison between SCIAMACHY tropospheric VCD (under two tropospheric NO_2 profile assumptions) and the VCD_{tropo_zenith}, for different cloud conditions. Bold values indicate the correlation coefficients between the satellite data and the NO_2 surface concentrations.

Cloud condition	80% of tropospheric NO_2 column located between 0–1 km			95% of tropospheric NO_2 column located between 0–1 km		
	R	Slope	Intercept	R	Slope	Intercept
All	0.68 **0.65**	0.54±0.06	−0.25±0.10	0.71 **0.58**	0.68±0.08	−0.20±0.14
Cloudy (CF>0.2)	0.58 **0.69**	0.30±0.07	−0.03±0.11	0.64 **0.74**	0.66±0.13	−0.32±0.20
Clear-sky (CF<0.2)	0.75 **0.62**	0.50±0.09	0.20±0.20	0.75 **0.59**	0.58±0.10	0.25±0.23
Clear-sky (CF<0.2, CTH>1 km)	0.86 **0.73**	0.50±0.12	0.15±0.33	0.83 **0.70**	0.56±0.14	0.30±0.42
Clear-sky (CF<0.2, CTH<1 km)	0.63 **0.64**	0.52±0.14	0.20±0.30	0.63 **0.66**	0.60±0.15	0.21±0.35

of data points, the correlation results should be treated with care and should be confirmed by additional studies in the future.

Figure 14c shows the comparison between tropospheric NO_2 VCDs from SCIAMACHY and zenith-sky measurements under clear-sky condition (CF<0.2). The data for days with CTH<1 km are also marked. The relative variations of the two data sets match well, while the absolute values of tropospheric NO_2 VCDs from zenith-sky measurements are 1.8±0.6 times as large as those retrieved from SCIAMACHY data.

Additionally, we investigate the correlation between the tropospheric NO_2 VCDs from SCIAMACHY measurements and the NO_2 surface concentrations measured by long-path DOAS observations, which have been used for satellite validation in previous studies (see e.g. Petritoli et al., 2004). As shown in Fig. 15, the correlation coefficient for data under clear-sky condition is 0.62 and that for data with CF<0.2 and CTH>1 km is 0.73, both of which are worse than the correlations between tropospheric NO_2 VCDs from SCIAMACHY and zenith-sky measurements. These findings also demonstrate the advantage of our VCD_{tropo_zenith} for satellite validation. The quality of satellite validation using surface concentration data will strongly depend on the time of the day and will be best for satellite instruments with overpass times during the noon.

4.2.3 Discussion

Unlike Sect. 3.1.4 and 3.1.5, which focus on the errors of the tropospheric NO_2 VCDs from zenith-sky measurements, in this section, the reasons for the deviation between data from SCIAMACHY and zenith-sky measurements are discussed, with the focus on the errors of the satellite data. In general, the most important sources of error in tropospheric NO_2 retrieved from SCIAMACHY data arise from the parameter settings in the calculation of tropospheric AMFs. Besides the errors caused by the determination of the stratospheric column and the surface albedo, which have been discussed in Richter and Burrows (2002), the different assumptions on the vertical and horizontal distribution of the tropospheric NO_2 column, as well as the aerosol single scattering albedo of satellite and zenith-sky AMF simulations also account for the deviation of the final comparison. Here it is interesting to note that the AMFs for satellite observations are more strongly affected by these assumptions, especially for (partly) clouded scenes. As mentioned before, the tropospheric AMFs used to deduce VCD_{tropo_zenith} are modeled under the assumption that all the tropospheric NO_2 is located within the PBL, which varies with different seasons. However, in the calculation of the SCIAMACHY AMFs, only 80% of the tropospheric NO_2 column is assumed to be located between 0–1 km altitude. In order to investigate the impact of such different assumptions, we re-calculate the tropospheric NO_2 VCDs from SCIAMACHY with 95% of the tropospheric NO_2 column located between 0–1 km. The results are mostly 15% larger than the old ones under clear-sky condition, with a few columns enhanced by a higher percentage. Thus, the absolute values of the new satellite tropospheric VCDs are closer to that of the VCD_{tropo_zenith}. The correlations between satellite tropospheric VCDs under these two distribution assumptions and the VCD_{tropo_zenith}, as well as the NO_2 surface concentrations from long-path DOAS measurements are presented in Table 3 for different cloud conditions. The correspondence between the tropospheric NO_2 VCDs from satellite and zenith-sky measurements is

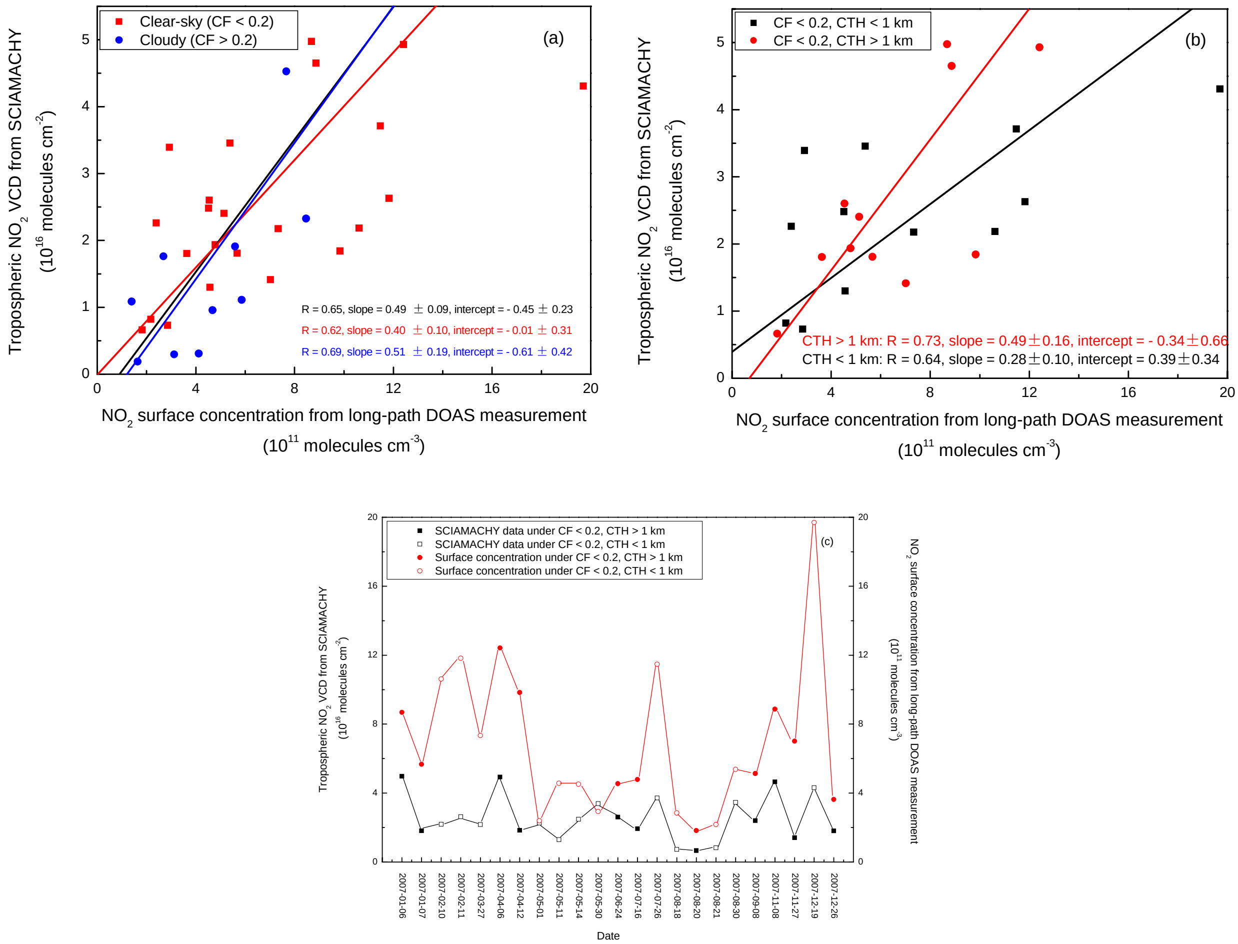

Fig. 15. Comparison between the tropospheric NO_2 VCDs deduced from SCIAMACHY and the NO_2 surface concentrations from long-path DOAS observations. **(a)** Orthogonal regression of the tropopheric NO_2 VCDs from SCIAMACHY and the NO_2 surface concentrations under all cloud fractions (the black fitted line). Red points represent the data for days under clear-sky condition, while the blue points represent the data for cloudy days; **(b)** Regression analysis of data for days with CF<0.2 & CTH<1 km (black points), and CF<0.2 & CTH>1 km (red points) respectively; **(c)** Time series of comparison between the tropospheric NO_2 VCDs from SCIAMACHY and NO_2 surface concentrations under clear-sky condition (CF<0.2). Open squares and circles represent the satellite VCDs and surface concentrations for days with CTH<1 km.

slightly improved by the use of the new profile assumption, but still cannot explain the major part of the deviation between the two data sets.

Additionally, as shown in Fig. 6c, the tropospheric AMFs deduced for an aerosol single scattering albedo of 0.95 are about 7% larger than those for a single scattering albedo of 0.9 (for the SZA of SCIAMACHY overpass, lower than 60°). Since 0.95 is probably the most realistic value of aerosol single scattering albedo, the derived tropospheric NO_2 VCDs from SCIAMACHY observations (with SSA assumed to be 0.9) are probably too high. Therefore, the correction of aerosol single scattering albedo settings would even enlarge the deviation between the two data sets. Again it should be noted that the effects of different aerosol settings are stronger for the satellite AMFs compared to the AMFs for zenith-sky observations.

After excluding the possibilities of the above two error sources as the main reasons for the deviation between satellite and zenith-sky tropospheric VCDs, we finally turn to the difference of spatial resolutions between the two measurements. According to Ordóñez et al. (2006), the agreement between the tropospheric NO_2 VCDs from satellite and ground-based in situ measurements in slightly polluted stations was better than that in heavily polluted or average polluted stations. Since our experimental site suffers from heavy traffic pollution, strong spatial gradients are to be expected, which cannot be resolved by the satellite observation. Thus the satellite observations should yield systematically lower

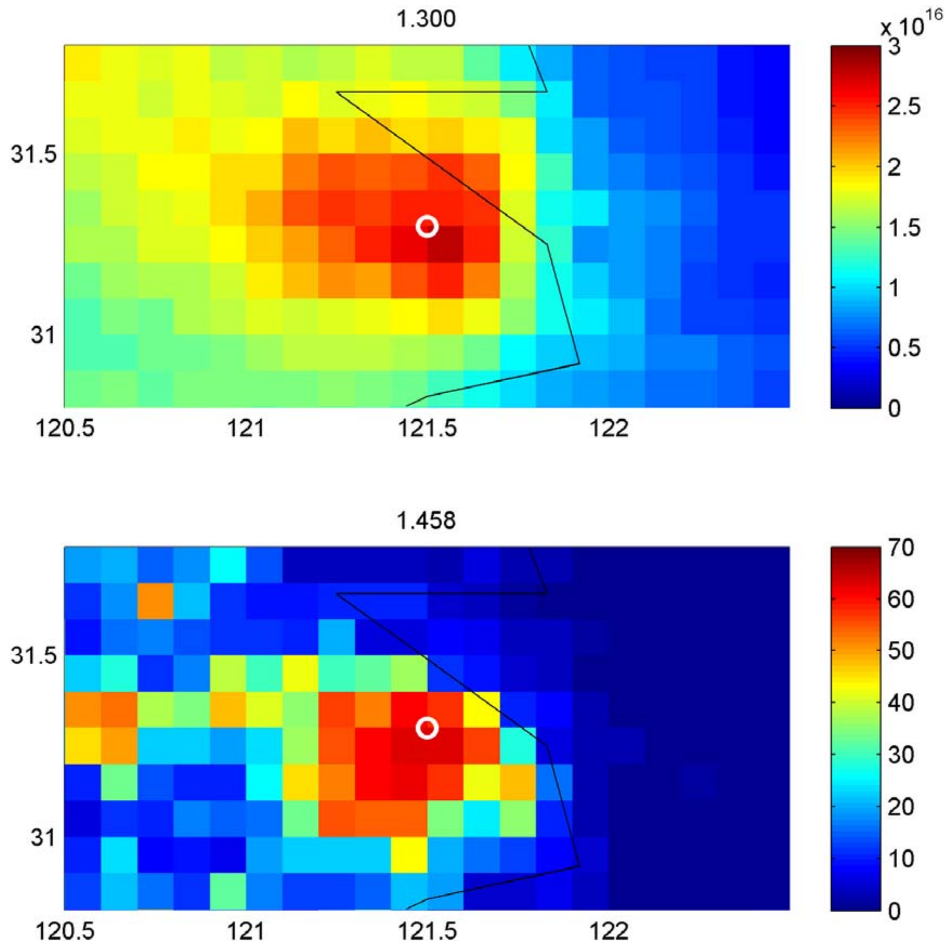

Fig. 16. Spatial distribution of NO_2 (top) and nighttime light pollution (bottom) around Shanghai. The NO_2 data are the average tropospheric VCDs from SCIAMACHY observations for 2007 with cloud fraction below 0.2. The nighttime light data are measurements from the "Defense Meteorological Satellite Program" DMSP-OLS. The numbers in the title gives the "spatial averaging effect", i.e. the ratio of the maximum at Shanghai and the mean of the satellite observations at a resolution of $30\times60\,km^2$. The circle indicates the ground-based experimental site. The black line represents the coastline of the East Sea.

values compared to those from zenith-sky measurements. In order to further demonstrate this effect, we investigate the spatial gradients around Shanghai to estimate the expected difference of zenith-sky versus satellite columns due to the extent of the satellite pixels ($30\times60\,km^2$). Figure 16 shows the spatial distribution of NO_2 and nighttime light pollution around Shanghai. The NO_2 data are the average tropospheric VCD from SCIAMACHY observations for 2007 with cloud fraction below 0.2. The nighttime light data are measurements from the "Defense Meteorological Satellite Program" DMSP-OLS for 2003 (Cinzano et al., 2001). The number in the title gives the "spatial averaging effect", i.e. the ratio of the maximum at Shanghai and the mean of the satellite observations at a resolution of $30\times60\,km^2$ (according to our selection criterion, see Sect. 4.2.1). Like for the NO_2 data themselves, the spatial averaging effect can also be quantified in a similar way for the nighttime light data. For the NO_2 measurements we find a ratio of 1.30, which can be regarded as the lower bound of the spatial sampling effect, because the NO_2 gradients were measured with the coarse spatial resolution of the satellite itself. In contrast, the light pollution at night might be a more realistic proxy for NO_x sources, as it was measured at higher spatial resolution. Hence, from the nighttime light pollution, we find a value of 1.46, which might be a good approximation of the upper bound of the spatial averaging effect. Therefore, the difference of zenith-sky versus satellite columns caused by spatial sampling effect ranges from 1.30 to 1.46, which can account for the main part of the deviation between the presented data sets.

Remaining systematic deviations are most probably related to uncertainties of the satellite data caused by the assumptions on the aerosol properties as well as layer heights of aerosols and NO_2. To sum up, considering the pollution level of the experimental site, the difference in the spatial resolutions of the satellite and ground-based observations, as well as the errors of both measurements, the present agreement level is rather good. In order to further validate the satellite measurement, it is necessary to extend the observation of zenith-sky DOAS measurement to the areas with different pollution levels to cover the whole footprint of the satellite measurements. Also more detailed information on the tropospheric NO_2 profile would decrease the uncertainties; such information could be e.g. derived from Multi-AXis- (MAX-) DOAS observations.

5 Conclusions

A new method to extract the tropospheric NO_2 VCDs from ground-based zenith-sky DOAS measurements is presented here. During a one year period, both zenith-sky scattered sunlight observations and long-path DOAS measurements were carried out simultaneously in Shanghai, China (31.3° N, 121.5° E). The former provide NO_2 total columns during daytime, while the latter provides information on NO_2 surface concentrations. By using a three-step strategy, the tropospheric NO_2 VCD was derived (VCD_{tropo_zenith}), which is an important quantity for the estimation of emissions and for the validation of satellite observations. A detailed error analysis shows that the accuracy of the tropospheric NO_2 VCDs derived by this extraction method is typically $<25\%$ for SZA below 70°.

The NO_2 surface concentrations measured by long-path DOAS were also converted into tropospheric VCDs ($VCD_{tropo\_surface}$) by multiplication with the assumed seasonal PBL heights. The comparison between the hourly-averaged $VCD_{tropo\_surface}$ and VCD_{tropo_zenith} provides a deeper insight on the influence of PBL height variation on the tropospheric NO_2 VCDs derived from the surface concentrations. It is concluded that the VCD_{tropo_zenith} is more reliable and suitable for satellite data validation.

A comparison between the tropospheric NO_2 VCDs from SCIAMACHY and zenith-sky measurements was made. The relative variations of the two data sets under clear-sky conditions (cloud fraction below 0.2) correspond well, while the absolute values of the VCDs from zenith-sky measurements are on average 1.8 times as large as those from SCIAMACHY observations. The best correlation is found for observations with $CF<0.2$ and $CTH>1$ km ($R=0.86$).

Reasons for the deviation of comparison results were explored, including the assumptions on the vertical and horizontal distributions of the tropospheric NO_2 concentration, the aerosol single scattering albedo, as well as the different spatial resolutions of the satellite and ground-based observations. It is concluded that the "spatial averaging effect" can account for a large part of the difference between zenith-sky and satellite observations. Since over Shanghai the distribution of pollution within the SCIAMACHY footprint shows typically strong and systematic gradients (with the maximum close to the measurement site of the ground-based observations), the satellite observations fail to reproduce the high NO_2 amounts over the polluted experimental site. Therefore, in order to further validate the satellite measurements, the extension of ground-based zenith-sky DOAS measurements is demanded to cover areas with different pollution levels within the whole satellite footprint.

Acknowledgements. We would like to thank the European Space Agency (ESA) operation center in Frascati (Italy) and the "Deutsches Zentrum für Luft- und Raumfahrt" (DLR, Germany) for making the satellite spectral data available. Information on effective cloud fraction and cloud top height was taken from the FRESCO algorithm (see http://www.temis.nl/fresco/fresco.html). We are also thankful for the planetary boundary layer height data provided by Patrick Jöckel from the Max-Planck-Institute for Chemistry, Mainz, Germany. Helpful discussions with Andreas Richter from the University of Bremen and Ulrich Platt from Heidelberg University are acknowledged. The radiative transfer calculations were performed using the TRACY-II model mainly developed in the satellite group of MPI, Mainz by Tim Deutschmann. The WinDOAS spectral analysis software was developed by Caroline Fayt and Michel van Roozendael in IASB/BIRA Uccle, Belgium. The McLinden climatology in SCIATRAN database used to calculate stratospheric NO_2 AMF is also acknowledged. The DMSP-OLS Nighttime Lights data were processed by NOAA's National Geophysical Data Center, and the DMSP data were collected by US Air Force Weather Agency. Finally, we are grateful to Howard Roscoe and other two anonymous reviewers for their positive and constructive reviews during the interactive discussion period of this paper.

Edited by: A. Richter

References

Bassford, M. R., McLinden, C. A., and Strong, K.: Zenith-sky observations of stratospheric gases: the sensitivity of air mass factors to geophysical parameters and the influence of tropospheric clouds, J. Quant. Spectrosc. Ra., 68, 657–677, 2001.

Beirle, S., Platt, U., Wenig, M., and Wagner, T.: Weekly cycle of NO_2 by GOME measurements: a signature of anthropogenic sources, Atmos. Chem. Phys., 3, 2225–2232, 2003, http://www.atmos-chem-phys.net/3/2225/2003/.

Beirle, S., Platt, U., Wenig, M., and Wagner, T.: Highly resolved global distribution of tropospheric NO_2 using GOME narrow swath mode data, Atmos. Chem. Phys., 4, 1913–1924, 2004, http://www.atmos-chem-phys.net/4/1913/2004/.

Boersma, K. F., Eskes, H. J., and Brinksma, E. J.: Error analysis for tropospheric NO_2 retrieval from space, J. Geophys. Res., 109, D04311, doi:10.1029/2003JD003962, 2004.

Bovensmann, H., Burrows, J. P., Buchwitz, M., Frerick, J., Noël, S., Rozanov, V. V., Chance, K. V., and Goede, A. P. H.:

SCIAMACHY: Mission Objectives and Measurement Modes, J. Atmos. Sci., 56(2), 127–150, 1999.

Brinksma, E. J., Pinardi, G., Braak, R., Volten, H., Richter, A., Schönhardt, A., van Roozendael, M., Fayt, C., Hermans, C., Dirksen, R. J., Vlemmix, T., Berkhout, A. J. C., Swart, D. P. J., Oetjen, H., Wittrock, F., Wagner, T., Ibrahim, O. W., de Leeuw, G., Moerman, M., Curier, R. L., Celarier, E. A., Knap, W. H., Veefkind, J. P., Eskes, H. J., Allaart, M., Rothe, R., Piters, A. J. M., and Levelt, P. F.: The 2005 and 2006 DANDELIONS NO_2 and aerosol intercomparison campaigns, J. Geophys. Res., 113, D16, doi:10.1029/2007JD008808, 2008.

Burrows, J. P., Dehn, A., Deters, B., Himmelmann, S., Richter, A., Voigt, S., and Orphal, J.: Atmospheric remote-sensing reference data from GOME: part 1. Temperature-dependent absorption cross sections of NO_2 in the 231–794 nm range, J. Quant. Spectrosc. Ra., 60(6), 1025–1031, 1998.

Burrows, J. P., Richter, A., Dehn, A., Deters, B., Himmelmann, S., Voigt, S., and Orphal, J.: Atmospheric remote-sensing reference data from GOME: part 2. Temperature-dependent absorption cross sections of O_3 in the 231–794 nm range, J. Quant. Spectrosc. Ra., 61, 509–517, 1999a.

Burrows, J. P., Weber, M., Buchwitz, M., Rozanov, V. V., Ladstätter-Weißenmayer, A., Richter, A., De Beek, R., Hoogen, R., Bramstedt, K., Eichmann, K. U., Eisinger, M., and Perner, D.: The Global Ozone Monitoring Experiment (GOME): Mission concept and first scientific results, J. Atmos. Sci., 56(2), 151–175, 1999b.

Cantrell, C. A.: Technical Note: Review of methods for linear least-squares fitting of data and application to atmospheric chemistry problems, Atmos. Chem. Phys., 8, 5477–5487, 2008, http://www.atmos-chem-phys.net/8/5477/2008/.

Celarier, E. A., Brinksma, E. J., Gleason, J. F., Veefkind, J. P., Cede, A., Herman, J. R., Ionov, D., Goutail, F., Pommereau, J.-P., Lambert, J. -C., van Roozendael, M., Pinardi, G., Wittrock, F., Schönhardt, A., Richter, A., Ibrahim, O. W., Wagner, T., Bojkov, B., Mount, G., Spinei, E., Chen, C. M., Pongetti, T. J., Sander, S. P., Bucsela, E. J., Wenig, M. O., Swart, D. P. J., Volten, H., Kroon, M., and Levelt, P. F.: Validation of Ozone Monitoring Instrument nitrogen dioxide columns, J. Geophys. Res., 113, D15S15, doi:10.1029/2007JD008908, 2008.

Cinzano, P, Falchi, F., and Elvidge, C. D.: The first world atlas of the artificial night sky brightness, Mon. Not. R. Astron. Soc., 328, 689–707, 2001.

Deutschmann, T. and Wagner, T.: TRACY-II Users manual, University of Heidelberg, 2006.

Duan, J. and Mao, J. T.: Study on the distribution and variation trends of atmospheric aerosol optical depth over the Yangtze River Delta, Acta Scientiae Circumstantiae, 27(4), 537–543, 2007.

EUMETSAT: GOME-2 Products Guide, http://oiswww.eumetsat.org/WEBOPS/eps-pg/GOME-2/GOME2-PG-index.htm, 2008.

Fayt, C. and v. Roozendael, M.: WinDOAS 2.1 software user manual, IASB/BIRA Uccle, Belgium, 2001.

Greenblatt, G. D., Orlando, J. J., Burkholder, J. B., and Ravishankara, A. R.: Absorption measurements of oxygen between 330 and 1140 nm, J. Geophys. Res., 95, 18577–18582, 1990.

Heue, K.-P., Richter, A., Bruns, M., Burrows, J. P., von Friedeburg, C., Platt, U., Pundt, I., Wang, P., and Wagner, T.: Validation of SCIAMACHY tropospheric NO_2-columns with AMAXDOAS measurements, Atmos. Chem. Phys., 5, 1039–1051, 2005, http://www.atmos-chem-phys.net/5/1039/2005/.

Hönninger, G. and Platt, U.: The role of BrO and its vertical distribution during surface ozone depletion at Alert, Atmos. Environ., 36, 2481–2489, 2002.

Institute of Remote Sensing University of Bremen: User's guide for the software package SCIATRAN (Radiative Transfer Model and Retrieval Algorithm), version 2.0, http://www.iup.uni-bremen.de/sciatran/downloads, Germany, 2004.

Ionov, D., Goutail, F., Pommereau, J.-P, and Bazureau, A.: Ten years of NO_2 comparisons between ground-based SAOZ and satellite instruments (GOME, SCIAMACHY, OMI), in: Proceedings of Atmospheric Science Conference, ESRIN, Frascati Italy, 8–12 May, 2006, published on CD-ROM., 16.1, 2006a.

Ionov, D., Sinyakov, V. P., and Semenov, V. K.: Validation of GOME (ERS-2) NO_2 vertical column data with ground-based measurements at Issyk-Kul (Kyrgyzstan), Adv. Space Res., 37(12), 2254–2260, 2006b.

Jöckel, P., Tost, H., Pozzer, A., Brühl, C., Buchholz, J., Ganzeveld, L., Hoor, P., Kerkweg, A., Lawrence, M. G., Sander, R., Steil, B., Stiller, G., Tanarhte, M., Taraborrelli, D., van Aardenne, J., and Lelieveld, J.: The atmospheric chemistry general circulation model ECHAM5/MESSy1: consistent simulation of ozone from the surface to the mesosphere, Atmos. Chem. Phys., 6, 5067–5104, 2006, http://www.atmos-chem-phys.net/6/5067/2006/.

Koelemeijer, R. B. A., Stammes, P., Hovenier, J. W., and de Haan, J. F.: A fast method for retrieval of cloud parameters using oxygen A band measurements from the Global Ozone Monitoring Experiment, J. Geophys. Res., 106, D4, 3475–3490, 2001.

Koelemeijer, R. B. A., Stammes, P., Hovenier, J. W., and de Haan, J. F.: Global distributions of effective cloud fraction and cloud top pressure derived from oxygen A band spectra measured by the Global Ozone Monitoring Experiment: Comparison to ISCCP data, J. Geophys. Res., 107, D12, 4151, doi:10.1029/2001JD000840, 2002.

Kraus, S.: DOASIS, DOAS for Windows software [CD-ROM], in: Proceedings of the 1st International DOAS-Workshop, Heidelberg, Germany, 2001.

Kühl, S., Puķīte, J., Deutschmann, T., Platt, U., and Wagner, T.: SCIAMACHY limb measurements of NO_2, BrO and OClO. Retrieval of vertical profiles: Algorithm, first results, sensitivity and comparison studies, Adv. Space Res., 42(10), 1747–1764, 2008.

Lambert, J. -C., Granville, J., Allaart, M., Blumenstock, T., Coosemans, T., De Mazière, M., Friess, U., Gil, M., Goutail, F., Ionov, D. V., Kostadinov, I., Kyrö, E., Petritoli, A., Piters, A., Richter, A., Roscoe, H. K., Schets, H., Shanklin, J. D., Soebijanta, V. T., Suortti, T., van Roozendael, M., Varotsos, C., and Wagner, T.: Ground-based comparisons of early SCIAMACHY O_3 and NO_2 columns, in: Proceedings of the First ENVISAT Validation Workshop, ESA/ESRIN, Frascati Italy, 9–13 December 2002, ESA SP-531, 2003.

Leue, C., Wenig, M., Wagner, T., Klimm, O., Platt, U., and Jähne, B.: Quantitative analysis of NO_x emissions from Global Ozone Monitoring Experiment satellite image sequences, J. Geophys. Res., 106, D6, 5493–5506, doi:10.1029/2000JD900572, 2001.

Levelt, P. F. and Noordhoek, R.: OMI Algorithm Theoretical Basis Document Volume I: OMI Instrument, Level 0-1b Processor, Calibration & Operations, Tech. Rep. ATBD-OMI-01, Version

1.1, August 2002.

Meena, G. S., Bhosale, C. S., and Jadhav, D. B.: Influence of tropospheric clouds on ground-based measurements of stratospheric trace gases at Tropical station, Pune, Atmos. Environ., 38(21), 3459–3468, 2004.

Noxon, J. F.: Nitrogen dioxide in the stratosphere and troposphere measured by ground-based absorption spectroscopy, Science, 189, 547–549, 1975.

Ordóñez, C., Richter, A., Steinbacher, M., Zellweger, C., Nüβ, H., Burrows, J. P., and Prévôt, A. S. H.: Comparison of 7 years of satellite-borne and ground-based tropospheric NO_2 measurements around Milan, Italy, J. Geophys. Res., 111, D05310, doi:10.1029/2005JD006305, 2006.

Perner, D. and Platt, U.: Absorption of light in the atmosphere by collision pairs of oxygen $(O_2)_2$, Geophys. Res. Lett., 7 (12), 1053–1056, 1980.

Petritoli, A., Bonasoni, P., Giovanelli, G., Ravegnani, F., Kostadinov, I., Bortoli, D., Weiss, A., Schaub, D., Richter, A., and Fortezza, F.: First comparison between ground-based and satellite-borne measurements of tropospheric nitrogen dioxide in the Po basin, J. Geophys. Res., 109, D15307, doi:10.1029/2004JD004547, 2004.

Pfeilsticker, K., Erle, F., Funk, O., Marquard, L., Wagner, T., and Platt, U.: Optical path modifications due to tropospheric clouds: Implications for zenith sky measurements of stratospheric gases, J. Geophys. Res., 103, D19, 25323–25335, 1998.

Platt, U.: Differential optical absorption spectroscopy (DOAS), in Air Monitoring by Spectroscopic Techniques, Vol. 127 of Chemical Analysis Series, edited by: Sigrist, M. W., John Wiley & Sons, Inc., New York, 1994.

Pommereau, J.-P. and Goutail, F.: O_3 and NO_2 ground-based measurements by visible spectrometry during arctic winter and spring 1988, Geophys. Res. Lett., 15, 891–894, 1988.

Puķīte, J., Kühl, S., Deutschmann, T., Platt, U., and Wagner, T.: Accounting for the effect of horizontal gradients in limb measurements of scattered sunlight, Atmos. Chem. Phys., 8, 3045–3060, 2008, http://www.atmos-chem-phys.net/8/3045/2008/.

Richter, A. and Burrows, J. P.: Tropospheric NO_2 from GOME measurements, Adv. Space Res., 29(11), 1673–1683, 2002.

Richter, A., Burrows, J. P., Nüß, H., Granier C., and Niemeier U.: Increase in tropospheric nitrogen dioxide over China observed from space, Nature, 437, 129–132, 2005.

Rothman, L. S., Rinsland, C. P., Goldman, A., Massie, S. T., Edwards, D. P., Flaud, J. -M., Perrin, A., Camy-Peyret, C., Dana, V., Mandin, J. -Y., Schroeder, J., McCann, A., Gamache, R. R., Wattson, R. B., Yoshino, K., Chance, K. V., Jucks, K. W., Brown, L. R., Nemtchinov, V., and Varanasi, P.: The HITRAN molecular spectroscopic database and HAWKS (HITRAN atmospheric workstation): 1996 edition, J. Quant. Spectrosc. Ra., 60(5), 665–710, 1998.

Solomon, S., Portmann, R. W., Sanders, R. W., Daniel, J. S., Madsen, W., Bartram, B., and Dutton, E. G.: On the role of nitrogen dioxide in the absorption of solar radiation, J. Geophys. Res., 104(D10), 12047–12058, 1999.

Vandaele A. C., Hermans, C., Simon, P. C., Carleer, M., Colin, R., Fally, S., Mérienne, M. F., Jenouvrier, A., and Coquart, B.: Measurements of the NO_2 absorption cross-section from 42 000 cm^{-1} to 10 000 cm^{-1} (238–1000 nm) at 220 K and 294 K, J. Quant. Spectrosc. Ra., 59, 171–184, 1998.

Van Roozendael, M., Hermans, C., De Mazière, M., and Simon, P. C.: Stratospheric NO_2 observations at the Jungfraujoch Station between June 1990 and May 1992, Geophys. Res. Lett., 21(13), 1383–1386, 1994.

Wagner, T., Erle, F., Marquard, L., Otten, C., Pfeilsticker, K., Senne, T., Stutz, J., and Platt, U.: Cloudy sky optical paths as derived from differential optical absorption spectroscopy observations, J. Geophys. Res., 103, D19, 25307–25321, 1998.

Wagner, T., von Friedeburg, C., Wenig, M., Otten, C., and Platt U.: UV-visible observations of atmospheric O_4 absorptions using direct moonlight and zenith-scattered sunlight for clear-sky and cloudy sky conditions, J. Geophys. Res., 107, D20, 4424, doi:10.1029/2001JD001026, 2002.

Wagner, T., Burrows, J. P., Deutschmann, T., Dix, B., von Friedeburg, C., Frieß, U., Hendrick, F., Heue, K.-P., Irie, H., Iwabuchi, H., Kanaya, Y., Keller, J., McLinden, C. A., Oetjen, H., Palazzi, E., Petritoli, A., Platt, U., Postylyakov, O., Puķīte, J., Richter, A., van Roozendael, M., Rozanov, A., Rozanov, V., Sinreich, R., Sanghavi, S., and Wittrock, F.: Comparison of box-air-mass-factors and radiances for Multiple-Axis Differential Optical Absorption Spectroscopy (MAX-DOAS) geometries calculated from different UV/visible radiative transfer models, Atmos. Chem. Phys., 7, 1809–1833, 2007, http://www.atmos-chem-phys.net/7/1809/2007/.

Wittrock, F., Oetjen, H., Richter, A., Fietkau, S., Medeke, T., Rozanov, A., and Burrows J. P.: MAX-DOAS measurements of atmospheric trace gases in Ny-Ålesund – Radiative transfer studies and their application, Atmos. Chem. Phys., 4, 955–966, 2004, http://www.atmos-chem-phys.net/4/955/2004/.

Yu, Y., Geyer, A., Xie, P., Galle, B., Chen, L. M., and Platt, U.: Observations of carbon disulfide by differential optical absorption spectroscopy in Shanghai, Geophys. Res. Lett., 31, L11107, doi:10.1029/2004GL019543, 2004.

Zhou, B., Hao N., and Chen, L. M.: Study on the effect of Fraunhofer structure to the measurement of atmospheric pollutants with differential optical absorption spectroscopy, Acta Phys. Sin-Ch Ed., 54(9), 4445–4450, 2005.